CHARACTERIZING THE EFFECT OF IONOSPHERIC DIVERGENCE ON DIFFERENTIAL GPS NAVIGATION

John Fabio Andreacchi, M.S.

Illinois Institute of Technology

Advisor: Dr. Boris Pervan

To further increase the accuracy of Differential GPS, the pseudorange and carrier phase measurements are brought together by means of a Hatch Filter to produce a smoothed pseudorange. The filter exploits the accuracy of the pseudorange and the precision of the carrier phase to mitigate multipath and other receiver associated noise. Among several errors embedded in the smoothed pseudorange, the one of interest in this paper is the filtered output of the Ionosphere induced group delay and phase advance. The carrier phase advance and pseudorange code (group) delay are equal and opposite. When filtered, an output error can exist depending on the input. In Differential GPS the errors will cancel completely between the reference and user filters only if they have the same time constants and have converged. The two cases considered here are when these conditions have not been met. Because the Ionosphere varies diurnally, seasonally, geographically and with solar activity, it is modeled using ramp, quadratic and sinusoidal inputs for each case. Typical values of observed ramp and quadratic behavior of the Ionosphere are .005 m/s and .000009 m/s^2 respectively. The most pronounced frequencies observed were approximately .001 Hz with varying amplitudes. The first case is when identical filters have different initialization times. Time domain analysis is sufficient to show the effects on the ranging error due to these inputs and yields bounding values for the "wait time" for filters before they can use corrections for any input

irrespective of its shape (using a .1 meter ranging error limit). The second case analyzed is when the ground and aircraft filters have same initialization times but mismatched time constants. In this case the ranging error will not cancel and its magnitude will depend on the magnitude and shape of the input. Time domain techniques as well as frequency domain techniques were used and from the results necessary and sufficient conditions to ensure the safe interoperability between filters in DGPS were defined. Treatment of Ionospheric divergence as a random process and applicability of stochastic analysis is also discussed.

CHARACTERIZING THE EFFECT OF IONOSPHERIC DIVERGENCE ON DIFFERENTIAL GPS NAVIGATION

BY

JOHN FABIO ANDREACCHI

Submitted in partial fulfillment of the
requirements for the degree of
Master of Science in Mechanical and Aerospace Engineering
in the Graduate College of the
Illinois Institute of Technology

Approved_____
Advisor

Chicago, Illinois
July 2000

ACKNOWLEDGMENT

I would like to thank my advisor, Dr. Boris Pervan, for giving me the opportunity and support to pursue this research. His advice and guidance, not only in satellite navigation, but also in research and academics, have been unmatched through every stage of my research. I would also like to thank Dr. Mohamad Tarabishy for input and assistance on many matters and Dr. John Way for his advice during the writing of this thesis.

I would like to thank my colleagues Moon Heo, Irfan Sayim and Fang-Chen Chan for their advice and support during the time of my research. I would also like to acknowledge the Federal Aviation Administration (FAA) for sponsoring my research.

I would like to thank my parents, Salvatore and Emma Andreacchi for their support and confidence in me throughout all of my academic life. Finally, I would like to thank my wife Elissa for her untiring help, encouragement and patience during my studies at Illinois Institute of Technology.

TABLE OF CONTENTS

LIST OF TABLES

LIST OF FIGURES

Figure Page

LIST OF SYMBOLS

Symbol	Definition
a_0	step coefficient
a_1	ramp coefficient
a_2	parabola coefficient
a_3	cubic coefficient
B_L	component of Earth's magnetic field parallel with radio wave
B_T	component of Earth's magnetic field perpendicular to radio wave
c	speed of light
c_ϕ	phase velocity
c_g	group velocity
δ	ranging error of single filter
$\Delta\delta$	differential ranging error
e	charge of an electron
ε_o	permittivity of free space
f	carrier frequency
ϕ	carrier phase measurement
Φ	Laplace transform of carrier phase measurement
I_s	Ionospheric delay for a particular satellite
I_{max}	maximum Ionospheric delay
I_{tol}	tolerable Ionospheric delay
k_o	initialization time difference

Symbol	Definition
κ	wave number
L1, L2	GPS carrier frequencies
λ	wave length of carrier frequency
m	mass of an electron
N	integer ambiguity
N_e	number of electrons
n_ϕ	refractive index for carrier
n_g	refractive index for modulation
ν	electron collision frequency
ν_ϕ	carrier multipath
ν_{pr}	code multipath
pr	pseudorange
PR	Laplace transform of smoothed pseudorange
r	Smoothed pseudorange
R	Laplace transform of smoothed pseudorange
ρ	true distance from user to satellite
T	sampling period
TEC	Total Electron Content
T_s	Tropospheric delay for a particular satellite
τ_a	aircraft filter time constant
τ_g	ground filter time constant
τ_s	satellite clock error

Symbol	Definition
τ_u	receiver clock error
$\Delta\tau$	difference in time constants between ground and aircraft filter
ω	carrier frequency in radians

CHAPTER I

INTRODUCTION

1.1 The Global Positioning System

Of the many techniques of determining ones location on this Earth, satellite navigation is the most sophisticated. The Global Positioning System (GPS) is the United States' radio-based, satellite navigation system for military and civil users alike. GPS provides global positioning capabilities for users 24 hours a day. The user finds his position by triangulation using the satellites as known reference points. There are three segments to the Global Positioning System. These segments are the space segment, the user segment and the control segment.

The space segment of the Global Positioning System is a constellation of 24 satellites that orbit the Earth with an altitude of approximately 20,000 km. There are four satellites in each of six orbit planes that have inclinations of 55 degrees. The satellites are in circular orbits with approximately 12 hour periods. This means they pass over the same location in the sky twice a day. This satellite constellation ensures the availability of GPS positioning 24 hours a day, anywhere on the Earth.

The user segment is the user's GPS receiver. Some of the less sophisticated GPS receivers of today are small enough to fit in one's pocket and can cost around $100. More sophisticated receivers can fit in a shoebox but may cost over $10,000 with a high quality antenna. The receivers obtain the location of the user by measuring the distance from the satellite to the user. These distances are measured by timing the travel of a radio message (signal) broadcast from the satellite to the receiver.

The last segment of the Global Positioning System is the control segment. The control segment is a network of monitoring stations strategically placed around the world and one master control station in Colorado Springs, Colorado. The orbiting satellites cannot stay in perfect orbits and furthermore cannot detect on their own if their orbit has been perturbed. The monitoring stations measure the locations of the satellites and send this data to the master control station. The master control station uses the information gathered from the monitoring stations and itself to develop corrections that are uploaded to the satellites.

With the high dependability of the space and control segments, and the small size and cost of the receivers, many practical applications for GPS currently exist. To name a few, GPS is used for location finding in the automotive, marine and aviation industries, and for people who travel on foot as well. When GPS is used in a more accurate, augmented form called Differential GPS (DGPS), it can be used for guidance and surveying. With the use of DGPS, progress is currently being made in guiding automotive, agricultural and aeronautic vehicles.

The proceeding sections will discuss GPS positioning and its associated errors, and how DGPS positioning can eliminate most of these errors. Finally, a method to make DGPS more accurate, called smoothing, and its implications will be discussed and the focus of this research will be defined.

1.2 GPS Positioning

As mentioned in the previous section a user can find his position by the measuring his distance from several satellites. There are nominally 24 satellites in GPS, but obtaining a

range from all satellites at one epoch is both unnecessary and impossible (because of visibility constraints). The minimum number of ranges needed to find one's location is four. If we let an unknown user's position be expressed in Earth Centered Earth Fixed (ECEF) coordinates (rotating Cartesian coordinates with origin at center of Earth), there are three unknown components to the user's position: x, y and z. To find a single location with these three unknowns, ranges from three known locations are needed. The fourth range is needed to solve for the receiver clock bias. Recall that the range from the satellite is found by measuring the transit time of the signal being broadcast. To measure this transit time the clock in the receiver must be synchronized with the clocks in all of the satellites. Because it is not practical to synchronize the receiver clock to the satellite clocks, the receiver clock bias is treated as an unknown, thus requiring the fourth range measurement to find the user's location. With four equations (ranges) the four unknown components of the user's position can be calculated.

For the user to measure his distance from the satellite, the satellite must continuously broadcast a signal recognizable by the receiver. The satellite broadcasts a navigation data message at 50 bps and Coarse Acquisition (C/A) code at 1.023 MHz, both modulated on a 1575.42 MHz carrier wave (L1). The satellites also broadcast a Precise (P) code at 10.23 MHz modulated on a 1227.6 MHz carrier wave (L2). The C/A code is for civil users while the P code is encrypted and not available to unauthorized users. When the signal is received the navigation data and C/A code are demodulated. In the navigation data, among other information, are the ephemerides of the satellite's orbit. From the ephemerides, the location of the satellite can be calculated at any given time. The distance from the (now known) location of the satellite is found by use of the C/A code.

The C/A code is input into a closed tracking loop called a Delay Lock Loop (DLL). In GPS receiver DLLs, an internally generated replica of the C/A code is compared with the received C/A code being broadcast by the satellites. Each satellite has its own unique C/A code. When the C/A code is received, the DLL will phase shift its replica until the correlation between the two signals is maximized. This phase corresponds to the time it took the signal to go from the satellite to the receiver (transit time). Since radio waves travel at the speed of light the range (distance) is found by multiplying the transit time by the speed of light.

$$c\Delta t = range \tag{1-1}$$

For this concept to work accurately, the clock that is used to generate the signal and the clock that is used to track the signal must be synchronized as mentioned above. The GPS satellites have very accurate and redundant atomic clocks that are very closely synchronized between each other. In contrast, typical receiver clocks use relatively inexpensive temperature-compensated crystal oscillators (TXCO) [Van95]. The term "relatively inexpensive" in used with respect to the cost of the satellite clocks. The receiver clock is one of the most expensive components in the receiver, but need be no better than a quartz oscillator.

1.3 GPS Errors

The range calculated by Equation (1-1), however, is not the true distance from the user to the satellite. There are six fundamental errors embedded in the range measurement so it is called the "pseudorange". The errors are listed below.

a. Satellite clock error

b. Satellite ephemeris error

c. Ionospheric delay

d. Tropospheric delay

e. Multipath

f. Receiver errors

To explain each of these errors, a signal will be traced from the moment it leaves the satellite to the moment it is received by the receiver.

The first errors actually occur before the signal is broadcast. They are the satellite clock error and the satellite orbit error. As mentioned previously the satellites have very accurate clocks generating the signals but there is still some error. These clock errors average from one to two meters [Park94]*. The ephemeris error is the second of the satellite errors. This is simply an error in the orbit determination of the satellite. There are three components to the orbit determination error: the radial, cross-track and along-track components. Observed values of the radial, cross-track and along-track components are 0.8 meters, 3.0 meters and 6.3 meters respectively [Zum94]. At zenith, the radial component of this error is the only one that contributes to the user's positioning error (the other components also contribute when not at zenith, but the radial component is the primary source).

The other errors occur after the signal has left the satellite, the first of which is induced by the Ionosphere. The Ionosphere is the upper section of the Earth's atmosphere, which contains free electrons and ions. When the signal propagates through the Ionosphere the modulation is delayed while the phase of the carrier is advanced. These phenomena are known as group delay and phase advance respectively and will be

discussed in detail in Chapter 2. The electrons and ions are produced by ultraviolet light and soft x-rays emitted by the sun. The Ionosphere contains four distinct, highly variable layers. The total electron content of the Ionosphere and the frequency at which the wave propagates through it affect the amount of delay. The delay due to the Ionosphere can be as high as 25 meters at the zenith. This error can be greater depending on the obliquity, or slant factor.

The second of the atmospheric errors is due to the Troposphere. The Troposphere is beneath the Ionosphere and delays the carrier and code both. The delay is caused primarily by water vapor and dry gases (O_2 and N_2). The Troposphere is also nondispersive (refractive index is constant with frequency) at the L1 and L2 frequencies so the carrier is delayed by the same amount as the code. Like the Ionosphere, the delay is increased with the obliquity factor. Taking the obliquity factor into account the delays due to the Troposphere can vary from 2 to 25 meters [Spil94], but can be more accurately modeled than the Ionosphere so such large delays are never seen.

Multipath is the next error of discussion. Consider the signal to be a planar wave front by the time it reaches the receiver. The correct pseudorange will be calculated from the ray of that wave front that is directly intercepted by the receiver. In reality this does happen but other rays of the wave front that bounce off the ground, trees or any nearby structure are received as well. This is called Multipath. The summation of all the received signals distorts the signal modulation and thus causes some error. Multipath signals are always late compared to the true pseudorange signal, but can result in either constructive or destructive interference. This induces a "noisy" error component that causes the pseudorange measurement to fluctuate in time. The size of the error depends

---

* Corresponds to coded reference in bibliography.

on the immediate environment, and the sophistication of the receiver (correlator spacing, antenna, etc.). Multipath affects both the code and carrier. Typical delays due to multipath are approximately one to two meters for the code and one centimeter for the carrier.

The last fundamental error to be discussed is receiver error. Receiver error is the combination of receiver precision, interchannel biases and thermal noise. The receiver precision is proportional to the wavelength the signal. For example, a typical precision of 1% of the wavelength results in an error on the C/A code of three meters while the error on the carrier would be .19 centimeters. As will be seen later, this high precision of the carrier phase measurements will be exploited to make the final range measurement more accurate. A standard model for the interchannel biases and thermal noise in modern receivers is a noise delay of 0.2 meters [Park94].

The rms combined error of the above error components can lead to a typical user range error of five to ten meters. This user error applies to the accuracy of the range between the user and a particular satellite. To obtain the user's actual position accuracy, the ranging accuracy must be multiplied by the Position Dilution of Precision (PDOP). The PDOP is a value that depends on the geometry of the constellation of satellites used at the time of the measurements. PDOP values can vary from about two to as high as six or seven [Park94]. With this in mind, the positioning accuracy of GPS is sufficient for a hiker wanting to find his location on a map, but for autonomously guiding land vehicles or aircraft, GPS accuracy must be improved.

1.4 Differential GPS

To make GPS more accurate, consider the errors in the range measurements that are common to receivers in close proximity to each other. The common errors are the satellite born errors and the atmosphere born errors. The satellite born errors are the satellite clock error and the orbit error. These are obviously common to receivers tracking the satellite in close proximity. The errors induced by the atmosphere are common because the satellite is so far away (20,000 km) compared to the distance between the receivers (50-100 km) that the signal effectively travels through the same atmospheric densities and variations at the same angle. This is true because the atmosphere is highly spatially correlated for short distances. Since these errors are common there is a way to cancel them between receivers leaving only noncommon errors to contend with. The noncommon errors are multipath and receiver error, which are environment and receiver specific respectively.

Differential GPS (DGPS) accomplishes just this. DGPS employs a reference station and a dynamic user receiver. The reference station is statically placed at a very accurately known location while the dynamic user can move about freely in some bounded perimeter (recall the receivers must be in close proximity). The purpose of the reference station is to calculate the error in a pseudorange measurement from a particular satellite then broadcast a correction via some communication link to a dynamic user. Dynamic users then use the corrections to get an accurate range from the same satellite. The reference station finds the error in the range measurement by using the fact that it already knows its position quite accurately. With its known position and the location of the satellite from the navigation message of the received signal, the reference station

calculates the time that it should take for the signal to reach its location from the satellite's location. Comparing this value with the time that it actually took the signal to reach the reference station is the ranging error for that particular satellite. Figure 1.1 shows potential accuracies of GPS and DGPS.

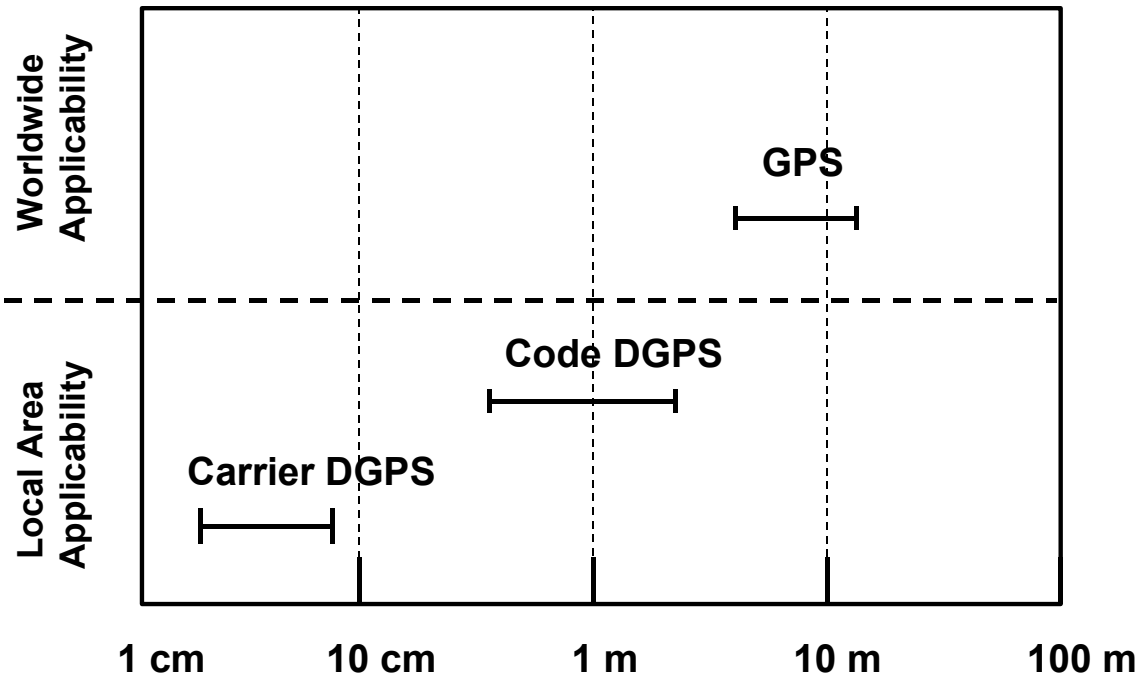

Figure 1.1 Potential Accuracies of GPS and DGPS

There are two kinds of DGPS presented: Carrier DGPS and Code DGPS. Carrier DGPS is very accurate but requires resolving the cycle integer ambiguity [Park95]. This kind of DGPS is used in surveying but may not be practical for real time applications.

In a Code DGPS (DGPS) system the range measurements are much more accurate than regular GPS but are still left with multipath and receiver error. These errors by themselves still provide an obstacle to using raw DGPS for precision landing of aircraft like in the Local Area Augmentation System (LAAS). However, the accuracy of the

range can be improved even further by using a filter to mitigate the fast multipath and receiver noise.

Consider the two curves in Figure 1.2. These curves are the pseudorange and the carrier phase measurements from a single satellite over some time period. The top curve is the pseudorange, which is noisy but provides an absolute measurement of distance. The bottom curve is the carrier phase, which is very precise but is only a relative measurement. The carrier phase measurement is found the same way as the pseudorange. Recall the pseudorange was found by running the C/A code through a Delay Lock Loop

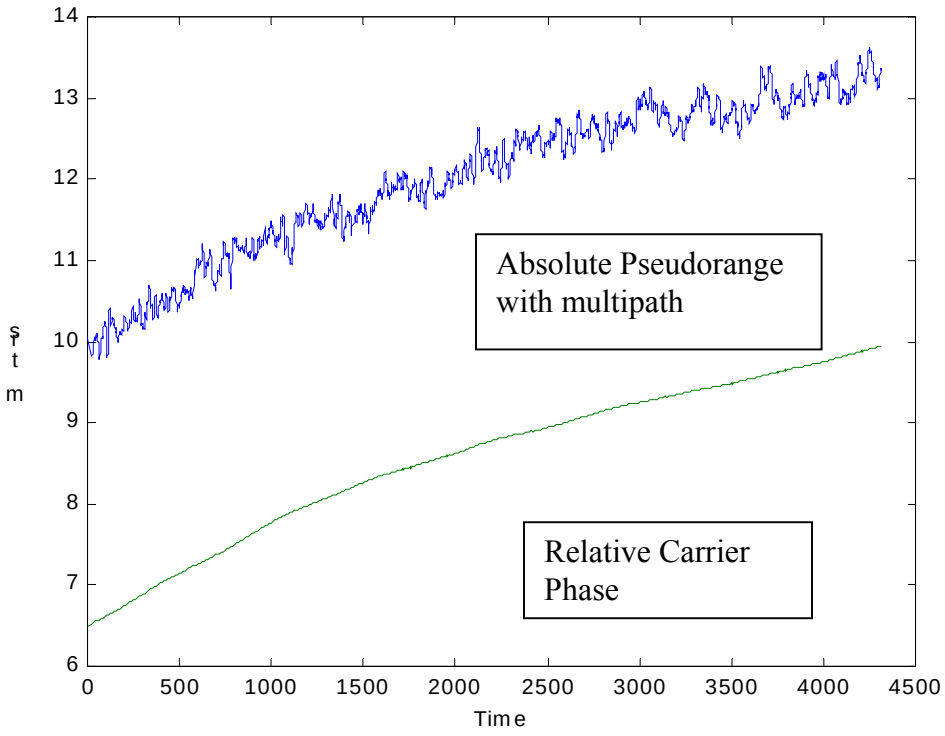

Figure 1.2. Pseudorange and Carrier Phase Measurements

(DLL). In contrast, the carrier phase range measurement is found by running the 1575.42 MHz carrier wave through a Phase Lock Loop (PLL). Since the carrier wave is just a raw

sinusoidal wave there are no distinguishing features to indicate the time it was broadcast. For this reason, there is a bias in the range measurement (not be confused with the receiver clock bias) that does not allow determination of the absolute range using the carrier phase alone. However, because it is much more precise than the C/A code, the carrier phase can be used to obtain a very accurate, relative measurements from epoch to epoch. The carrier phase measurement suffers from the same errors as the pseudorange obtained from the C/A code with the following exceptions: The multipath on the carrier phase is much less (multipath is proportional to the wavelength). The error due to the Ionosphere is equal but has an opposite effect on the carrier phase in that it advances the signal instead of delaying it. Finally, there is an additional offset in the carrier phase measurement called the cycle integer ambiguity. This is the range bias mentioned earlier that disables the carrier phase measurement from being an absolute range.

The absolute nature of the pseudorange and the precision of the carrier phase are brought together to produce a "smoothed pseudorange" by using a smoothing filter. The smoothing filter is a recursion that effectively shifts the carrier phase curve up (in Figure 1.2) until it is centered on the pseudorange curve. The output of the filter, the smoothed pseudorange, is a weighted combination of the raw pseudorange, the carrier phase and the previous smoothed pseudorange measurement. An implication that arises with a smoothing filter of this type is due to the Ionosphere. As noted just above, the Ionosphere causes a delay in the pseudorange and an advance in the carrier phase. These effects are called "group delay" and "phase advance", respectively. As the Ionosphere changes density, the group delay and phase advance change proportionally, causing divergence between the code and carrier phase measurements. The origin of this effect

will be discussed in detail in the next chapter. The presence of Ionospheric divergence impedes the smoothing of the pseudorange in a DGPS system if the right conditions are not met.

The purpose of this research is to characterize the effect of Ionospheric divergence on DGPS ranging, and define sufficient and necessary conditions for the safe interoperability between reference and user filter implementations with respect to Ionospheric Divergence. Chapter 2 will present how the Ionosphere changes with time and a derivation of group delay and phase advance. Chapter 3 will derive the particular smoothing filter used in a DGPS implementation and introduce potential output errors as a function of the input. The remaining chapters contain the analyses performed on the filters using different models for Ionospheric Divergence. The summary chapter will use all the results produced by the analyses to define sufficient and necessary conditions. These conditions have direct applicability to the ongoing development of the Local Area Augmentation System (LAAS). LAAS is an architecture that uses DGPS to land aircraft autonomously.

.

CHAPTER II

THE IONOSPHERE

2.1 The Ionosphere

As mentioned previously the Ionosphere is the upper part of the Earth's atmosphere that contains free electrons and ions. The free electrons and ions are produced by Ultraviolet (UV) light and X-ray emissions from the sun ionizing primarily O_2 and N_2. Recombination of these ions and electrons occurs at night but is very slow so a number of these pairs still exist at sunrise. The electron and ion densities are approximately equal so the net charge is equal to zero. This assumption is known as charge neutrality. The Ionosphere has a lower limit of 50 to 70 km but has no distinguishable upper limit. The vertical structure of the Ionosphere continuously changes thoughout the day, from season to season and with latitude. Solar activity influences the Ionosphere as well. The Ionosphere has four layers at varying heights. In increasing peak altitude and electron concentration, the layers are D, E, F1 and F2. Each layer is distinguishable by the their difference in physical processes. One particular process that differs at each layer is the absorption characteristic. Because the ultraviolet light and x-ray emissions are partially blocked from one layer to the next, ionization occurs at different rates and for different durations. Other differing processes like recombination and actual atmosphere composition are a product of atmospheric density and altitude respectively [Tas94]. Table 2.1 shows each layer and their electron contents. As can be seen in Table 2.1, the D and F1 regions vanish at night and the E region becomes very weak. The F2 region diminishes continuously but still possesses a considerable electron density by sunrise, when the ionization process starts again.

Table 2.1. Ionospheric Layers and Their Electron Content

Region	Altitude (km)	N_e peak (cm^{-3})	
D	90	$1.5e10^4$	day
		0	night
E	110	$1.5e10^5$	day
		$<1e10^4$	night
F1	200	$2.5e10^5$	day
		0	night
F2	300	10^6	day
		10^5	night

2.2 Ionosphere Variability

The variability of the Ionosphere is actually the variability of the total electron content. This variability can be characterized as normal variations and non-normal variations. Normal variations are the diurnal, seasonal, spatial and solar cycle variations. The diurnal variation is a swell of high electron content with its peak occurring at 2:00 pm local time. The seasonal variation is described as the mean electron content of the layers of the Ionosphere changing throughout the year. The seasonal variation is seen in the E and F1 layers because their electron contents are higher in the summer than in the winter. This is opposite for the F2 layer. The Ionosphere has a high amount of electron content in the equatorial anomaly and auroral zones and lower at other latitudes. The equatorial anomaly is a region described as 15 degrees north and south of the magnetic equator. At this region the Ionosphere contains the highest electron content worldwide [Dor97]. The solar cycle is an 11 year cycle measured by the amount of UV light

emitted by the Sun. As explained earlier, the UV light produces the electrons and ions in the Ionosphere, so the electron content will vary with this 11 year cycle.

Non-normal variations are those that are unpredictable and depend mainly on solar activity. These variations stem from Sudden Ionospheric Disturbances (SID), Polar Cap Absorption (PCA) and geomagnetic storms. The Sudden Ionospheric Disturbance is appears soon after a strong solar flare. Its existence is described by increases in electron content in the D and lower E layers caused by x-ray penetration. A SID may only last for an hour or so. Polar Cap Absorptions are seen only in the polar regions and happen more gradually than SIDs and have longer durations. PCAs occur when energetic protons from a solar flare finally arrive at the Earth and are guided by the Earth's magnetic field lines to the polar caps. As a result, the high energy of the protons ionize atoms in the lower E and D. A PCA can last for several days. The geomagnetic storm is also a result of solar flares. It starts about 20 hours after a solar flare and is associated higher electron contents in the E and D layers. These storms differ from PCAs in that they are most intense at night.

Models for the normal variations of the Ionosphere have been developed to partially correct for the errors induced by the Ionosphere. Of the least complex is the monthly mean model, which is simply a constant value. This model has been shown to correct for approximately 50% of the error. A better model for Ionosphere, which effectively mimics the diurnal variation of the Ionosphere is the "half cosine" model developed by Klobuchar [Klob86] often used in single frequency GPS receivers. This model is allowed to vary in amplitude and period and with user latitude. These models were developed to use minimal computational resources in a GPS receiver but only account for normal

variations. Because of the non-normal variations, it is considered impossible to model the Ionosphere to better than 75% accuracy [Klob96].

2.3 Group Delay and Phase Advance

In the previous chapter it was stated that the free electrons in the Ionosphere induce the phenomenon known as group delay and phase Advance. group delay is when the modulation envelope of some radio signal is delayed, while phase advance is when the carrier wave of that signal is advanced. To see how this is possible consider the equation for a wave,

$$\phi_1 = \cos\omega\left(t - \frac{x}{c_\phi}\right) \tag{2-1}$$

where $\omega = 2\pi f$, x is the distance from the satellite and c_ϕ is the velocity of the carrier wave. If we let $\lambda_\phi = c_\phi / f$ be the wave length and the wave number be $\kappa = 2\pi / \lambda_\phi$, Equation (2-1) can be rewritten as

$$\phi_1 = \cos(\omega t - \kappa x) \tag{2-2}$$

Now consider a second wave with a slightly different ω and κ.

$$\phi_2 = \cos[(\omega + \Delta\omega)t - (\kappa + \Delta\kappa)x] \tag{2-3}$$

The superposition of Equations (2-2) and (2-3), and the use of trigonomic identities, the resultant equation is an equation for a modulated radio signal.

$$\phi_s = \phi_1 + \phi_2 = 2\cos\frac{1}{2}(\Delta\omega t - \Delta\kappa x)\cos\left[\left(\omega + \frac{\Delta\omega}{2}\right)t - \left(\kappa + \frac{\Delta\kappa}{2}\right)x\right] \tag{2-4}$$

This equation is analogous the equation of the C/A code modulated on the L1 carrier wave. The first cosine term in Equation (2-4) represents the C/A code modulation and

the second cosine term represents the carrier wave with frequency L1. Comparing the first cosine term of Equation (2-4) with Equation (2-1), we can see that the velocity of the modulation, or the group velocity, is

$$c_g = \frac{\Delta\omega}{\Delta\kappa} \tag{2-5}$$

Taking the limit as Δω and Δκ approach zero, the differential form of the group velocity is

$$c_g = \frac{d\omega}{d\kappa} \tag{2-6}$$

The group and phase velocities can be related to their refractive indicies by the following expression.

$$c = c_g n_g = c_\phi n_\phi \tag{2-7}$$

Where c is the speed of light in a vacuum and n_g and n_ϕ are the refractive indicies of the modulation and carrier waves respectively. First, consider the refractive index for the carrier wave, n_ϕ. Since the Ionosphere is dispersive, n_ϕ depends on the frequency of the carrier wave. This refractive index can be derived from the equations of motion of an electron is an electromagnetic field and Maxwell's equations. The result is Appleton's formula [Dav65]:

$$n_\phi{}^2 = 1 - \frac{X}{1 - iZ - \frac{Y_T^2}{2(1 - X - iZ)} \pm \left[\frac{Y_T^4}{4(1 - X - iZ)^2} + Y_L^2 \right]^{\frac{1}{2}}} \tag{2-8}$$

where

$X = Ne^2/\varepsilon_o m\omega^2$
$Y_L = eB_L/m\omega$
$Y_T = eB_T/m\omega$
$Z = \nu/\omega$

$\omega = 2\pi f$
f = carrier frequency
N = number of electrons
e = charge of an electron
ε_o = permittivity of free space
m = mass of an electron
B_L = component of Earth's magnetic field parallel with radio wave
B_T = component of Earth's magnetic field perpendicular with radio wave
ν = electron collision frequency

A first order approximation of Appleton's formula can be found by ignoring the effect of the Earth's magnetic field and collisions of electrons and higher order terms to yield [Lei95]:

$$n_\phi = 1 - X \tag{2-9}$$

To find n_g as a function of n_ϕ, substitute Equation (2-6) into (2-7) and solve for n_g.

$$n_g = c\frac{d\kappa}{d\omega} \tag{2-10}$$

Substituting the wave number of the carrier in for κ and some manipulation yields

$$n_g = c\frac{d}{d\omega}\left(\frac{2\pi}{\lambda}\right) = \frac{d}{d\omega}\left(\frac{c}{\lambda f}2\pi f\right) = \frac{d}{df}\left(\frac{c}{\lambda f}f\right) \tag{2-11}$$

Executing the differentiation, and recognizing that the first term in the differential is the refractive index of the carrier wave, the refractive index for the modulation becomes

$$n_g = n_\phi + f\frac{dn_\phi}{df} \tag{2-12}$$

The final expression for the group refractive index is found by substituting Equation (2-9) in (2-12) to give

$$n_g = 1 - X + f\frac{d(1-X)}{df} = 1 + X \tag{2-13}$$

The phase and group velocities are then found by substituting the expressions for the refractive indicies in Equation (2-7) and ignoring the higher order terms.

$$c_g = \frac{c}{1+X} \approx c(1-X) \tag{2-14}$$

$$c_\phi = \frac{c}{1-X} \approx c(1+X) \tag{2-15}$$

By inspection of the above equations, the velocities of the carrier phase and group deviate from the speed of light in a vacuum by equal and opposite amounts which is given by

$$\Delta c = cX \tag{2-16}$$

The value X is always a positive number for very high frequencies, like L1 and L2, that pierce through the Ionosphere. From this derivation the phase velocity of the carrier wave exceeds the speed of light. This may seem to violate the theory of relativity but actually does not because there is no information, or energy, be transmitted faster than c. The energy is actually slightly delayed (group delay).

The connection between the Ionosphere and the signal velocities is the density of electrons along the path of the signal as it leaves the satellite and is received by the receiver. The unit by which this electron density is measured by is called the Total Electron Content (TEC). It is the number of electrons in an imaginary column having a cross sectional area of $1m^2$ and extending from the satellite to the receiver. Δc is found by substitution of physical values for X in Equation (2-15) to give

$$\Delta c = \frac{40.3c}{f^2} N \tag{2-17}$$

Integrating the number of electrons in a $1m^2$ area from the time it takes the signal to get from the satellite to the user yields:

$$I = \frac{40.3c}{f^2} \int_{receiver}^{satellite} N dt \tag{2-18}$$

To find the delay or advance in meters, by integrating N over the path from the satellite to the user, use the following relationship derived from Equations (2-14) or (2-15).

$$dt = \frac{1}{c}(1 \pm X) ds \tag{2-19}$$

Substituting (2-19) into (2-18) and again ignoring higher order terms the Ionospheric delay/advance is

$$I_s = \frac{40.3}{f^2} \int_{receiver}^{satellite} N ds = \frac{40.3}{f^2} TEC \tag{2-20}$$

The values of the group delay and phase advance are the same but the group delay is effectively added to the pseuodrange measurement and the phase advance is subtracted from the carrier phase measurement. When the electron densities in the Ionosphere change as a result of any of the previously mentioned Ionospheric variations, the group delay and phase advance will vary proportionally. The equal and opposite change of these values this is called Ionospheric Divergence. The proceeding chapters study how this divergence affects the output of the smoothing filter, which uses both the pseudorange and carrier phase measurements as inputs.

CHAPTER III

THE HATCH FILTER

3.1 The Hatch Filter

The digital filter typically used for smoothing the pseudorange measurement to mitigate multipath and other receiver associated noise is the Hatch Filter [Hat82]. The Hatch Filter is a dual input single output filter, the inputs are the pseudorange (code) and the RF carrier phase (carrier) and the output is the smoothed pseudorange. The code provides an absolute measure of the range between the user and the satellite, but is obscured with multipath noise. The carrier is much more precise than the code because the multipath error on the inputs is proportional to their wavelengths. However, because of the cycle ambiguity, it is a relative measurement. The Hatch filter brings together the absolute, but noisy, pseudorange measurement with the very precise, but relative, carrier phase measurement for a smoothed pseudorange measurement that is free of high frequency multipath (correlation time less than the time constant). The discrete implementation of the filter is,

$$r(k) = \frac{N-1}{N}\left[r(k-1) + \phi(k) - \phi(k-1)\right] + \frac{1}{N}\,pr(k) \tag{3-1}$$

where

r(k) = Smoothed Pseudorange
ϕ(k) = Carrier Phase Measurement
pr(k) = Raw Pseudorange Measurement
N = τ/T
τ = Filter Time Constant
T = Sampling Period

The continuous Hatch filter can be obtained by taking the limit of Equation (3-1) as T approaches zero:

$$\tau\dot{r}(t) + r(t) = \tau\dot{\phi}(t) + pr(t) \tag{3-2}$$

Taking the Laplace transform and solving for R(s) yields

$$R(s) = \frac{\tau s\Phi(s) + PR(s)}{\tau s + 1} \tag{3-3}$$

A derivation, of how a generic first order filter is actually implemented to suppress the multipath noise, is now shown.

Consider the equations for the pseudorange and carrier phase measurements:

$$pr = \rho + (\tau_u + \tau_s)c + T_s + I_s + \nu_{pr} \tag{3-4}$$

$$\phi = \rho + (\tau_u + \tau_s)c + T_s - I_s + \lambda N + \nu_\phi \tag{3-5}$$

where

pr= Pseudorange measurement
ϕ = Carrier Phase measurement
ρ = true range
τ_u = error due to receiver clock offset
τ_s = error due to satellite clock offset
T_s = delay from Troposphere
I_s = delay from Ionosphere
λ = Wavelength of Carrier Wave
N = Integer Ambiguity
ν_{pr} = code multipath
ν_ϕ = carrier multipath

The equations have the same true ranges, clock errors and Tropospheric delays. The multipath on each is different as mentioned previously. The errors due to the Ionosphere, are equal and opposite. It is understood that the Ionosphere causes a delay in the pseudorange, but the negative sign preceding it in the carrier phase implies that it is actually an advance rather than a delay. This is the group delay and phase advance

discussed in Chapter 2. The extra term, *N*, in the carrier phase measurement is called the integer ambiguity. It accounts for the bias in distance between carrier phase measurement and the true range. If we subtract Equation (3-4) from (3-5) we are left with an expression called code-minus-carrier (CMC).

$$pr - \phi = 2I - \lambda N + \nu_{pr-\phi} \tag{3-6}$$

The CMC is the cycle ambiguity plus twice the Ionospheric delay and CMC mutlipath. The objective of the Hatch filter is to attenuate multipath and receiver noise from the pseudorange measurement. By transforming Equation (3-6) to the Laplace domain and applying a first order filter,

$$\frac{1}{\tau s + 1} \tag{3-7}$$

we are left with a filtered estimate of the integer cycle number ($\hat{N}$) plus filtered Ionospheric delay and noise terms.

$$\frac{PR(s) - \Phi(s)}{\tau s + 1} = -\lambda \hat{N} + \frac{2I(s)}{\tau s + 1} + \frac{\nu_{pr-\phi}}{\tau s + 1} \tag{3-8}$$

This estimate of the integer cycle can be used to provide an absolute measurement between the user and the satellite. If we combine Equation (3-8) with the raw carrier phase measurement, Equation (3-5), we obtain the following result:

$$R(s) = \frac{PR(s) - \Phi(s)}{\tau s + 1} + \Phi(s) = \frac{2I(s)}{\tau s + 1} - I(s) + \frac{\nu_{pr-\phi}}{\tau s + 1} + \nu_{\phi} + \rho(s) + (\tau_r + \tau_s)c + T(s) \tag{3-9}$$

Among the true distance, ρ, there are other errors in the filter output (smoothed pseudorange). The clock errors and Tropospheric delay will be cancelled when the filter is used in a DGPS scheme. The multipath terms will not cancel but are filtered out to some extent. In particular, slow varying multipaths (with correlation times above the

time constant of the recursion) will not be filtered out and will contribute to the differential ranging error. Unlike the Troposphere delay, the Ionosphere delay is filtered by the recursion. Depending on the dynamics of the Ionosphere and the specific filter implementations, there may be a residual ranging error. Given certain conditions this error will cancel when used in a DGPS scheme. When these conditions are not met, the errors will not cancel and hence a differential ranging error exists. With some manipulation of the left side of Equation (3-9), it can be shown to be identical to Equation (3-3), the continuous Hatch Filter.

3.2 Ranging Error of the Hatch Filter

Because the Hatch Filter is a linear, first order filter there will be, in general, some ranging error in the output due to Ionospheric divergence. The error will depend on how the divergence is characterized (first, second and third order input). In this analysis we will consider only the Ionospheric effect on the smoothed pseudorange, which reduces Equation (3-9) to

$$R(s) = \rho(s) + \frac{-I(s)\tau s + I(s)}{\tau s + 1} \tag{3-10}$$

By inspection, the second term on the right side of Equation (3-10) is the simply the Hatch filter with the Ionosphere as its input instead of the carrier phase and pseudorange. The negative Ionosphere term represents the carrier phase advance and the positive Ionosphere term represents the pseudorange group delay. From Equation (3-10) the transfer function from Ionospheric input to ranging output is

$$\frac{R(s)}{I(s)} = -\frac{\tau s - 1}{\tau s + 1} \tag{3-11}$$

This term yields a negative value for increasing Ionospheric divergence rates. For convenience it will be multiplied by –1 since only the magnitude of the error is of interest. This is a first order, type zero filter, so there will be a steady state error for a first order input. This steady state ranging error for a single filter is calculated by subtracting the input (group delay on pseudorange) from the output (filtered Ionospheric divergence). Recall that the group delay on the pseudorange is now represented by –I(s) from the sign change made earlier.

$$\delta(s) = I(s)\frac{\tau s - 1}{\tau s + 1} - \left(-I(s)\right) \tag{3-12}$$

Simplifying and factoring out the Ionosphere term, the function for the ranging error in the s-domain is

$$\delta(s) = I(s)\frac{2\tau s}{\tau s + 1} \tag{3-13}$$

Letting the Ionosphere be represented by a ramp function (first order curve),

$$I(s) = \frac{a_1}{s^2} \tag{3-14}$$

and applying the final value theorem to Equation (3-14), the steady state error for the single filter is simply

$$\delta_{ss} = \lim_{s\to 0} s\frac{a_1}{s^2}\frac{2\tau s}{\tau s + 1} = 2a_1\tau \tag{3-15}$$

It is easily seen that the steady state ranging error is proportional to the time constant of the filter and the rate of constant change of the Ionospheric divergence. Equations (3-14) and (3-15) are illustrated in the time domain response to a ramp divergence in Figure 3.1.

If the Ionospheric divergence behaves like a parabolic or higher order curve then the ranging error will not settle to a steady state value. Instead, it will continue to grow for as

long as the rate of change of the Ionosphere sustains a parabolic or higher order shape. This is shown in Equation (3-16) by letting the Ionospheric divergence input be a parabola and applying the final value theorem.

$$\delta_{ss} = \lim_{s\to 0} s \frac{2a_2}{s^3} \frac{2\tau s}{\tau s + 1} = \infty \tag{3-16}$$

From above, it is obvious that the ranging error grows indefinitely since the final value equals infinity.

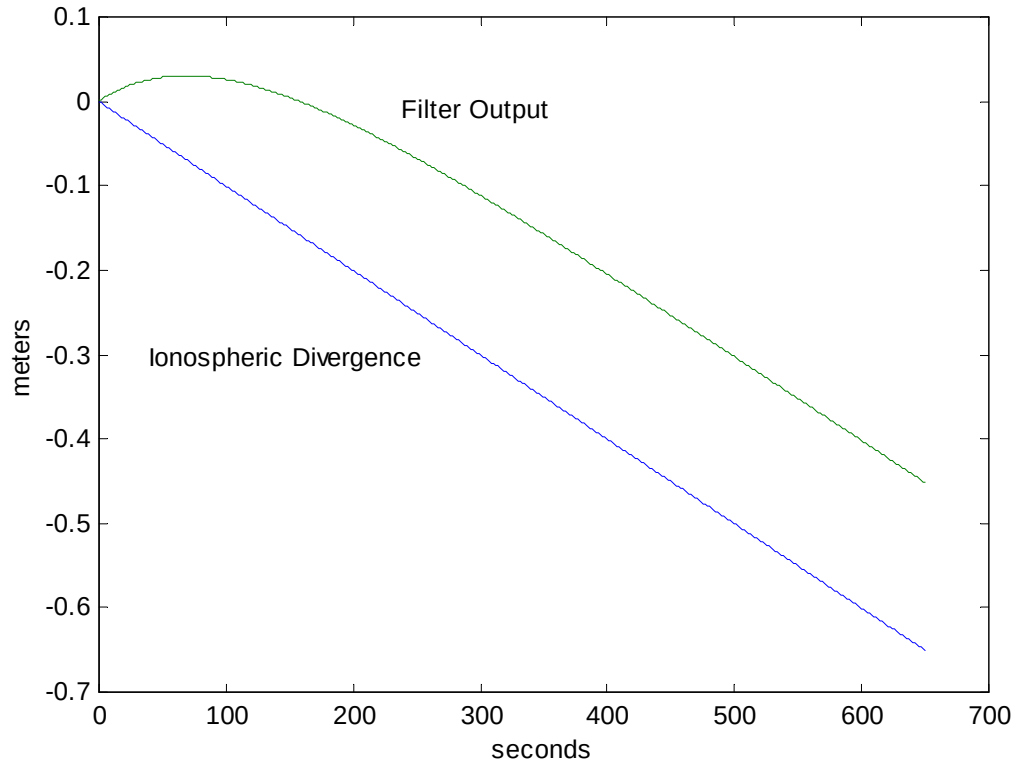

Figure 3.1. Ionospheric Divergence Characterized as a Ramp Function and the Response of the Hatch Filter

Figure 3.2 shows the response of the Hatch filter to a parabolic input. From these plots, it is clear that the ranging error can get quite large. For an epoch when the Ionosphere diverges quickly, it may seem that the resulting ranging error is larger than the multipath

error itself, thus defeating the original intention of the Hatch filter. However, in a DGPS implementation like LAAS, there are two receivers using Hatch filters whose outputs are differenced. If the filters are identical (same time constants), and reached steady state the ranging errors will cancel. If the filters are not the same then there will be a differential ranging error. This differential ranging error for a ramp input is found by differencing (3-15) with itself but using different time constants,

$$2a_1\left(\tau_g - \tau_a\right) \tag{3-17}$$

where τ_g is the time constant of the ground reference station and τ_a is the time constant of the aircraft. For higher order divergence rates the differential ranging error will grow if the ground and air filters are different. Depending on the magnitude, the differential ranging error can pose a threat to the integrity of the LAAS system. Preliminary work by the Radio Technical Committee on Aeronautics (RTCA) suggests that differential ranging errors less than .1 meters due to Ionospheric divergences may be tolerable [MOP99]. The Federal Aviation Administration (FAA) has also required that the ground filter have a time constant of 100 seconds, but no specific requirement has been set on the aircraft filter [FAA99]. In the upcoming chapters the behavior of the differential ranging error will be analyzed for several given scenarios. It is the intention of this analysis to alert LAAS aircraft receiver manufacturers of the effects of the Ionosphere on smoothing filters with different initialization times or mismatched time constants in the ground and aircraft filters. The difference in initialization time affects the validity of the broadcasted correction for receivers that have just begun tracking satellites. Time constant mismatches can cause differential ranging error for the whole time corrections are used.

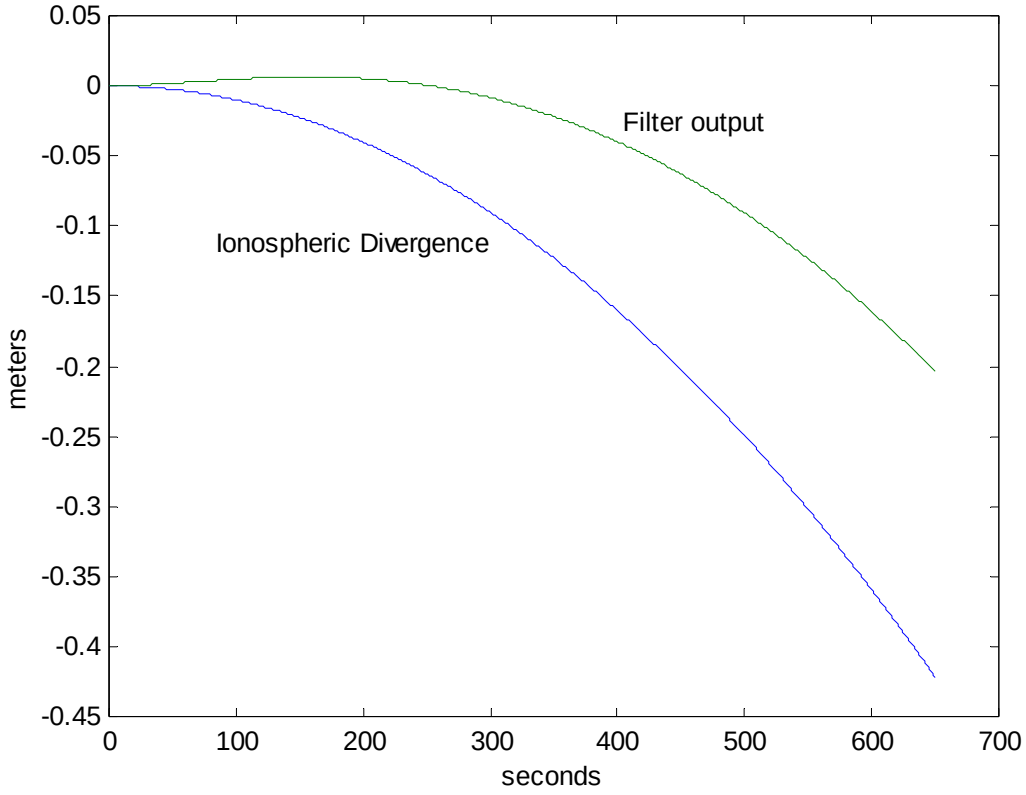

Figure 3.2. Ionospheric Divergence Characterized as a Parabolic Function and the Response of the Hatch Filter

CHAPTER IV

ANALYSIS WITH INITIALIZATION TIME DIFFERENCE

4.1 Analytic Solution to Hatch Filter

This analysis is performed using two identical Hatch filters (same time constants) that are initialized at different times. It is done in two ways, first theoretically and then experimentally. Using the theoretical approach enables us to come to certain conclusions about the behavior of the filters somewhat quickly. The experimental results will be combined with the analytical results to form meaningful statements and suggestions for the Hatch filter implementation in LAAS. To start the theoretical analysis, the solution of the Hatch filter difference equation is found by first taking its z-transform.

$$R(z)z - r_o z = \frac{N-1}{N}\left[R(z) + \Phi(z)z - \phi_o z - \Phi(z)\right] + \frac{1}{N}\left[PR(z)z - p_o z\right] \tag{4-1}$$

If we make the following substitutions,

$$\begin{aligned} r_o &= p_o = -a_o \\ \phi_o &= a_o \\ PR(z) &= -I(z) \\ \Phi(z) &= I(z) \end{aligned} \tag{4-2}$$

Equation (4-1) can be represented in terms of the Ionospheric divergence rate and its initial conditions.

$$R(z) = I(z)\left[\frac{(\tau - 2T)z - \tau + T}{\tau z - z + T}\right] - \frac{2a_o z(\tau - T)}{\tau z - z + T} \tag{4-3}$$

To find a solution an input must be applied to the transfer function. The input will be the Ionospheric divergence. Since the divergence rate itself varies with time we begin with a model of Ionospheric divergence as a third order polynomial in time.

$$i(kT) = a_o + a_1 kT + a_2 (kT)^2 + a_3 (kT)^3 \tag{4-4}$$

Taking the z-transform of the above equation yields

$$I(z) = a_o \frac{z}{z-1} + a_1 \frac{Tz}{(z-1)^2} + a_2 \frac{T^2 z(z+1)}{(z-1)^3} + a_3 \frac{T^3 z(z^2+4z+1)}{(z-1)^4} \tag{4-5}$$

Combining (4-3) and (4-5) and taking the inverse z-transform leaves the general solution to the Hatch filter.

$$r(k) = -a_o + A_0 \left[\left(\frac{\tau - T}{\tau} \right)^k - 1 \right] + A_1 k + A_2 k^2 + A_3 k^3 \tag{4-6}$$

$$\begin{aligned}
A_0 &= a_3 (2T^3 - 14T^2\tau + 24\tau^2 T - 12\tau^3) + a_2 (2T^2 - 6T\tau + 4\tau^2) + a_1 (2T - 2\tau) \\
A_1 &= 6a_3 (-T^3 + 3T^2\tau - 2T\tau^2) + 4a_2 (-T^2 + T\tau) - a_1 T \\
A_2 &= 6a_3 (-T^3 + T^2\tau) + a_2 (-T^2) \\
A_3 &= a_3 (-T^3)
\end{aligned}$$

In this analysis we assume the ground receiver has locked on to a satellite before the aircraft receiver has. To define appropriate initial conditions we assume the Ionoshperic delay at t=0 is zero because we are interested in the rate of change of the Ionosphere and not its absolute magnitude at a certain point in time. The ground filter's initial conditions will always be zero. Initial conditions for the aircraft filter must be calculated from the divergence Equation (4-4) and the difference in initialization times of the filters (denoted by k_o). For the same input, there may be initial conditions for the aircraft depending on the aircraft initialization time. When the input is first order (a_2=a_3=0), the only additional initial condition needed at the aircraft is a bias (or step) to compensate for the value of the Ionosphere at the time the aircraft filter initializes. This is found simply by evaluating the first order input function at k_o.

$$a_o = a_1 k_o T \tag{4-7}$$

For a second order input (a_1=a_3=0) the rate is not constant but increases with time. To account for this, two additional initial conditions must be imposed at the aircraft. Again there will be a bias or step initial condition to compensate for the value of Ionospheric delay at aircraft initialization given by

$$a_o = a_2 (k_o T)^2 \tag{4-8}$$

The other is a first order (or ramp) initial condition to compensate for the initial rate of change at aircraft initialization. The ramp initial condition is the slope of the input and is found by differentiating the input and evaluating it at k_o.

$$a_1 = 2 a_2 k_o T \tag{4-9}$$

The appropriate initial conditions are substituted and the solution of the differential ranging error can be found by differencing Equation (4-6) for the ground filter and aircraft filter respectively.

4.2 Response to Ramp Input

The first case considers a ramp input for the Ionospheric divergence model.

$$i(kT) = a_1 kT \tag{4-10}$$

Using (4-7) in (4-6) and differencing the ground and aircraft solutions, the differential ranging error becomes

$$\Delta\delta = a_1 \left[2(\tau - T) \left[\left(\frac{\tau - T}{\tau} \right)^{k-k_o} - \left(\frac{\tau - T}{\tau} \right)^{k} \right] \right] \tag{4-11}$$

Figure 4.1 shows an example ramp divergence rate with the ground and air filters tracking it. The filters have an initialization time difference $k_o T$=200. The difference of the two filter outputs, Equation (4-11) is shown in Figure 4.2.

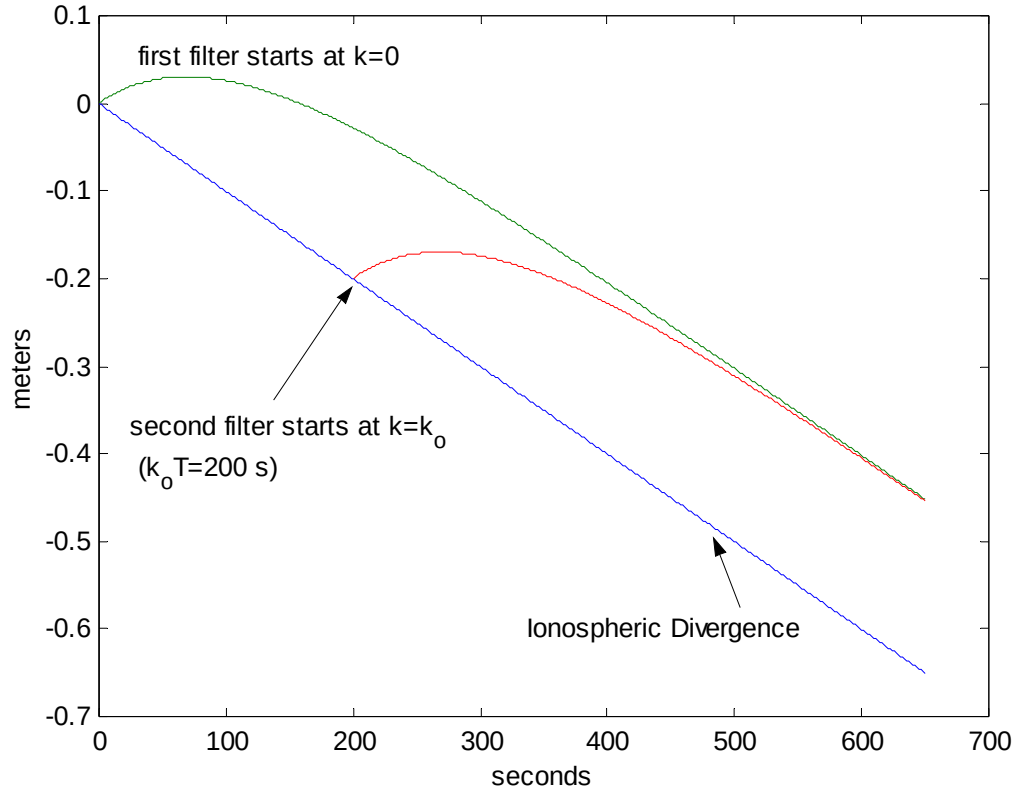

Figure 4.1. Ramp Ionospheric Divergence Rate being Tracked by Ground and Aircraft Filters with Different Initialization Times

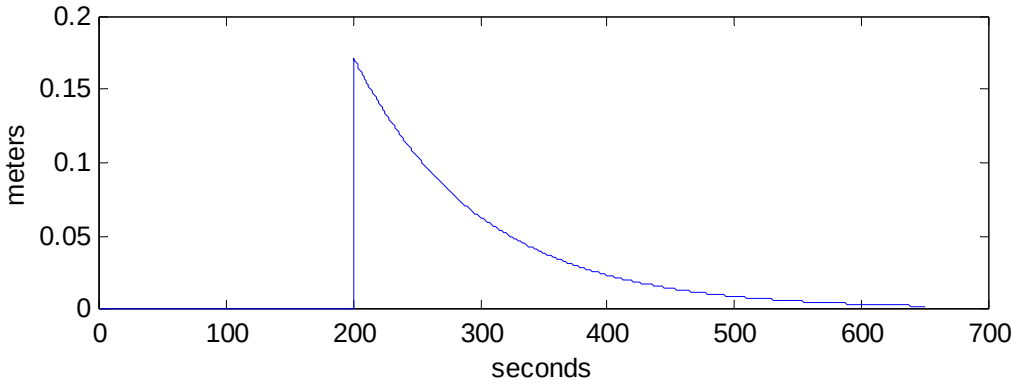

Figure 4.2. Differential Ranging Error Between Ground and Aircraft Filters

To facilitate a better understanding of Equation (4-11), it can be parameterized and put in the form,

$$\frac{\Delta\delta}{a_1\tau} = 2\left(1-\frac{T}{\tau}\right)\left(1-\frac{T}{\tau}\right)^{\frac{kT}{\tau}\frac{\tau}{T}}\left[\left(1-\frac{T}{\tau}\right)^{\frac{-k_oT}{\tau}\frac{\tau}{T}}-1\right] \qquad (4\text{-}12)$$

and plotted for different initialization times (Figure 4.3).

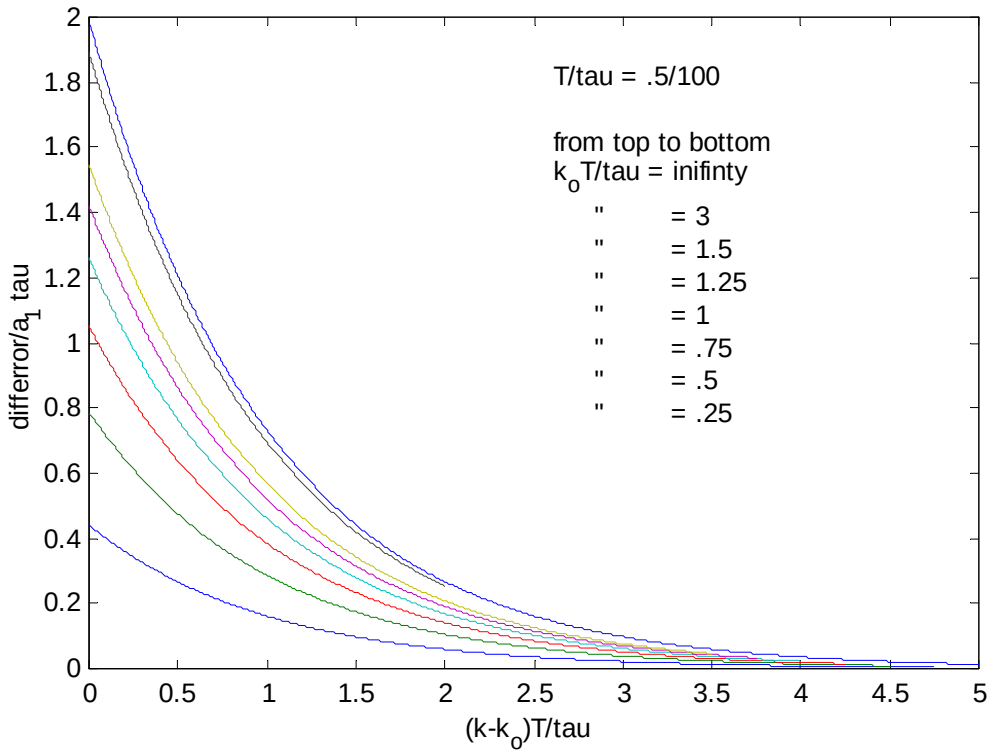

Figure 4.3. Parameterized Curves for Ramp Divergence with Varying Initialization Times

The top-most curve in Figure 4.3 represents a difference in initialization time (k_o) that is infinity. This corresponds to the aircraft filter initializing when the ground filter is already at steady state. In this situation the differential ranging error starts at the aircraft filter's steady state error value and decays to zero (as the filter converges). After the

aircraft filter converges, the differential ranging error is zero because they are identical filters with identical inputs.

One of the utilities of Figure 4.3 is that the time to wait, after the one filter has initialized, may be defined such that the differential ranging error is less than some specified safety limit for a given constant divergence. When the safety limit has been reached, the aircraft can use the corrections being broadcast by the ground filter. For example, assume the given parameters of a particular situation are a 100 second time constant, .5 second sampling period, a differential ranging error limit of .1 meters and a constant divergence rate of .01 meters/second [MOP99]. To suggest a wait time that is suitable for all values of k_o, the worst case initialization difference of infinity will be used (one filter has reached steady state). The parameterized differential ranging error is

$$\frac{\Delta\delta}{a_1\tau} = \frac{.1m}{(100s)(.01m/s)} = .1 \tag{4-13}$$

The value of kT/τ which yields this for the k_oT/τ=infinity curve is the parameterized wait time for a constant divergence rate input.

From Figure 4.4 we see that the parameterized wait time has a value of approximately 3. The actual wait time is calculated by multiplying the 3 by the time constant of the filter, which gives

$$\frac{(k-k_o)T}{\tau}\tau = 300 \quad \text{seconds} \tag{4-14}$$

This implies that an aircraft wait 300 seconds after it is locked on to a satellite, before the differential ranging error with the ground filter is within its specified limit. This also applies when the aircraft filter starts to track before the ground filter. The analysis just

conducted was for a constant divergence rate only, but this value will be a benchmark for analysis of higher order divergence inputs.

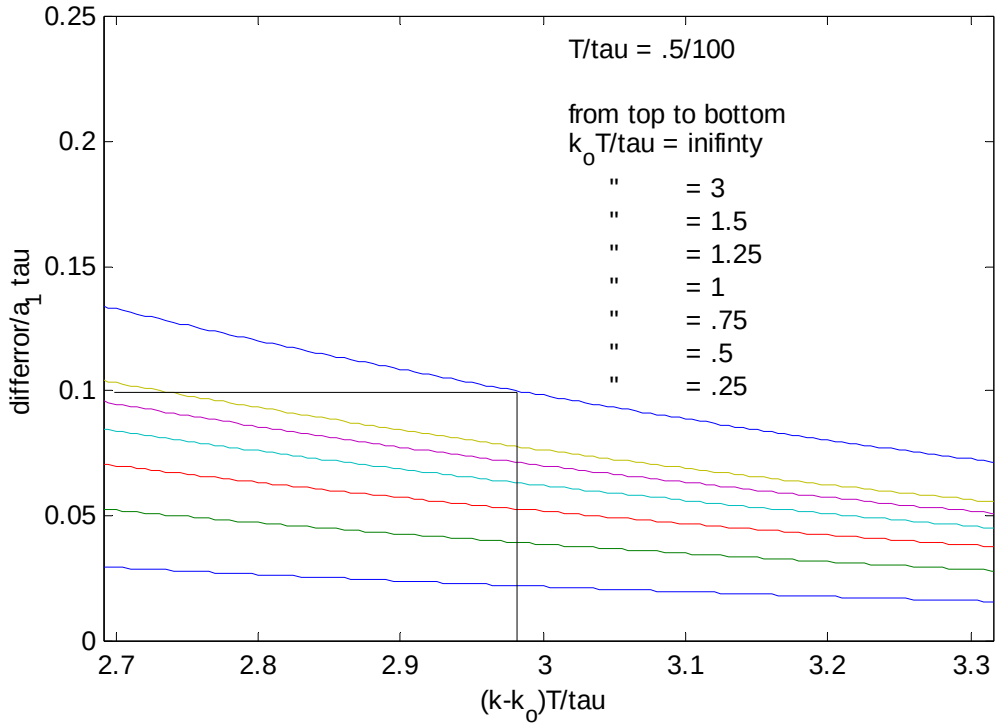

Figure 4.4. Wait Time for Filters using 100 second Time Constant, Infinite Initialization Time Difference and .01 m/s Divergence Rate

4.3 Response to Parabolic Input

There are times when the Ionospheric divergence rate is not well modeled by a first order curve but better modeled by higher order curves. In this regard, second order inputs are considered next. The solution to the differential ranging error with a second order input is found using the same approach as was used for Equation (4-11). Substituting the appropriate initial conditions, the solution is

$$\Delta\delta = a_2\left[2(\tau - T)(T - 2\tau)\left[\left(\frac{\tau - T}{\tau}\right)^{k-k_o} - \left(\frac{\tau - T}{\tau}\right)^{k}\right] + 4(\tau - T)k_o T\left(\frac{\tau - T}{\tau}\right)^{k-k_o}\right] \quad (4\text{-}15)$$

Recall that the ranging error for a single filter will increase for as long as a second or higher order input is sustained. Because of this fact, there will not be a worst case

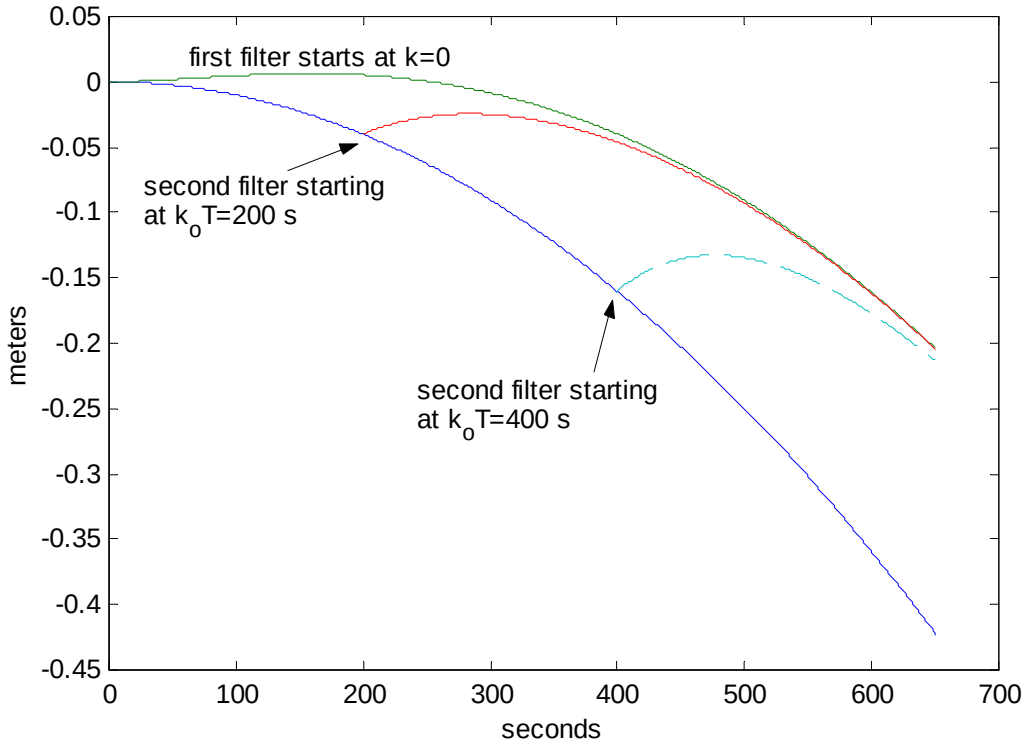

Figure 4.5. Second Order Ionospheric Divergence with Filters Tracking It

differential initialization time k_o. Instead as k_o increases, the initial differential ranging error will increase as well. Notice in Figure 4.5, when the first filter initializes at kT=0 and the second filter initializes at k_oT=200 s, the initial differential ranging error is about -.05 meters. However, when the second filter initializes at k_oT=400 s, the initial differential ranging error is about -.11 meters. For now, we will use the 300 second wait

time found in the previous section to find a tolerable coefficient for a second order input (a_2 from Equation (4-4)) and corresponding initialization difference k_o. This is accomplished by parameterizing Equation (3-15),

$$\frac{\Delta\delta}{a_2\tau^2} = 2\left(1-\frac{T}{\tau}\right)\left(\frac{T}{\tau}-2\right)\left(1-\frac{T}{\tau}\right)^{\frac{kT}{\tau}\frac{\tau}{T}}\left[\left(1-\frac{T}{\tau}\right)^{\frac{-k_oT}{\tau}\frac{\tau}{T}}-1\right]+\ldots$$
$$4\left(1-\frac{T}{\tau}\right)k_o\frac{T}{\tau}\left(1-\frac{T}{\tau}\right)^{\left(\frac{kT}{\tau}-\frac{k_oT}{\tau}\right)\frac{\tau}{T}} \qquad (4\text{-}16)$$

and plotting several curves for different values of k_o.

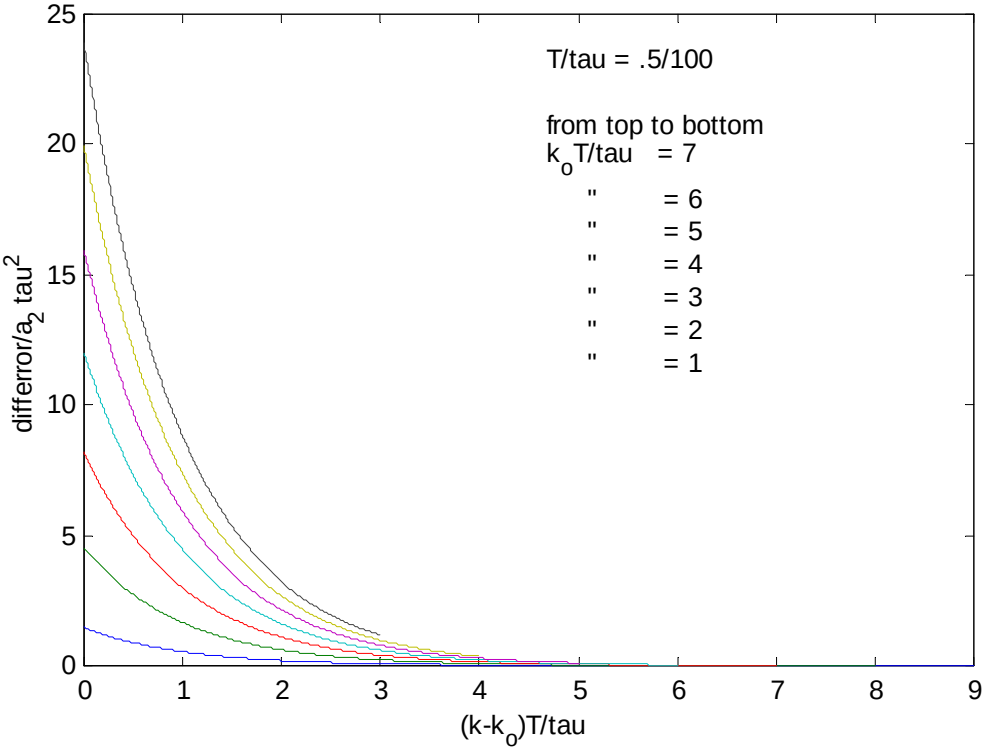

Figure 4.6. Parameterized Curves for Parabolic Divergence with Varying Initialization Times

There is no worst case curve on this plot in that an infinite number of curves actually exist. To show this, let a line be drawn vertically from $(k-k_o)T/\tau = 3$ point on the horizontal axis. The points where this line intersects the k_oT/τ curves correspond to tolerable values of the parameterized safety limit. In this situation, as the initialization time difference k_o increases, the size of the parabolic input must decrease to stay within the specified differential error limit in $(k-k_o)T = 3\tau$ seconds. Vice versa, if the size of the parabolic input increases, then the initialization time must decrease to keep the differential error within specified limits for a given wait time $(k-k_o)T/\tau$. This is different than the ramp analysis because there is no bounding initialization time difference. For this reason the initialization time difference and the size of the parabola, a_2, must be known to use this plot.

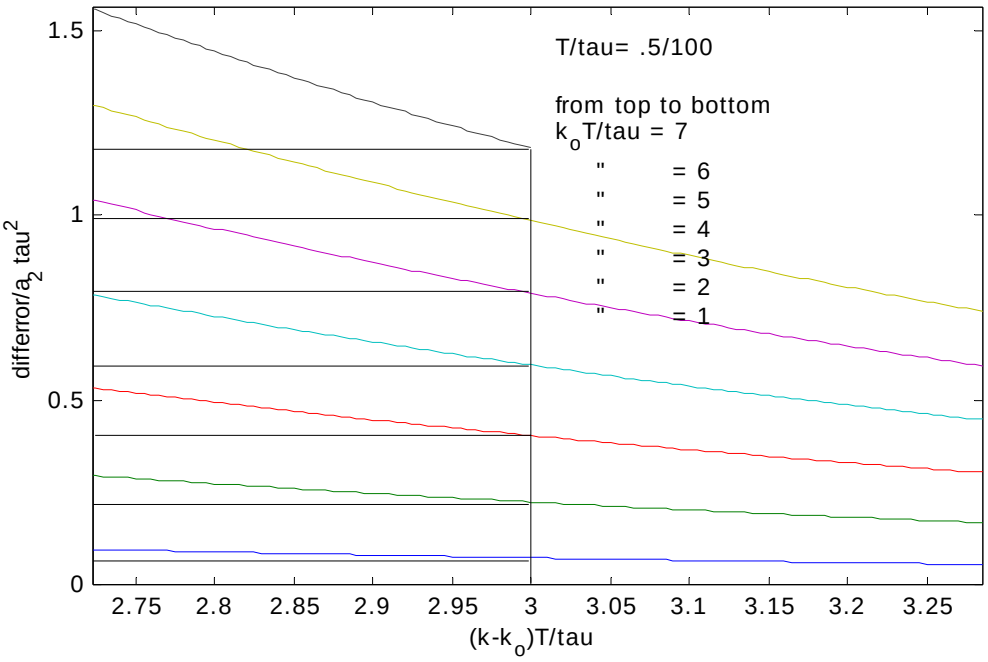

Figure 4.7. Different Combinationa of the Parameterized Safety Limit and a_2 for a 300 Second Wait Time

It is important to note however, that a parabolic model, or any higher order polynomial model, does not by itself accurately model the Ionosphere. This is true because the Ionosphere is bounded and the polynomials are not. The Ionosphere is bounded because there is an absolute limit on how much delay the Ionosphere can induce. By this assumption we can deduce that parabolas (or inputs of first order or higher) can only be sustained for as long as it takes to reach this maximum value. When the Ionospheric delay finally reaches this maximum value it can take one of two actions. First, it can stay at that value in which case it can be modeled as a step input. The second action that can be taken is the rate changes directions and the magnitude of the delay begins to decrease. This type of behavior can be modeled by a sinusoidal input. If an approximation of a parabolic input by a sinusoidal input can be established then the results found in the sinusoidal analysis will apply to the parabolic input case. The approximation is found by using a sinusoidal Ionospheric input equation with a maximum absolute delay of 25 meters given by

$$i(kT) = \frac{I_{\max}}{2}\left(1 - \cos(\omega_I kT)\right) \tag{4-17}$$

Expanding the cosine to its two first terms an approximation is uncovered.

$$a_2(kT)^2 = \frac{I_{\max}\omega_I}{4}(kT)^2 \tag{4-18}$$

The approximation is plotted with the sinusoid in Figure 4.8 and shows that the approximation fits fairly well up to $\pi/2\omega$ seconds. This mathematical relationship will let the results of the sinusoidal input apply to parabolic input. The frequency analysis will be conducted next.

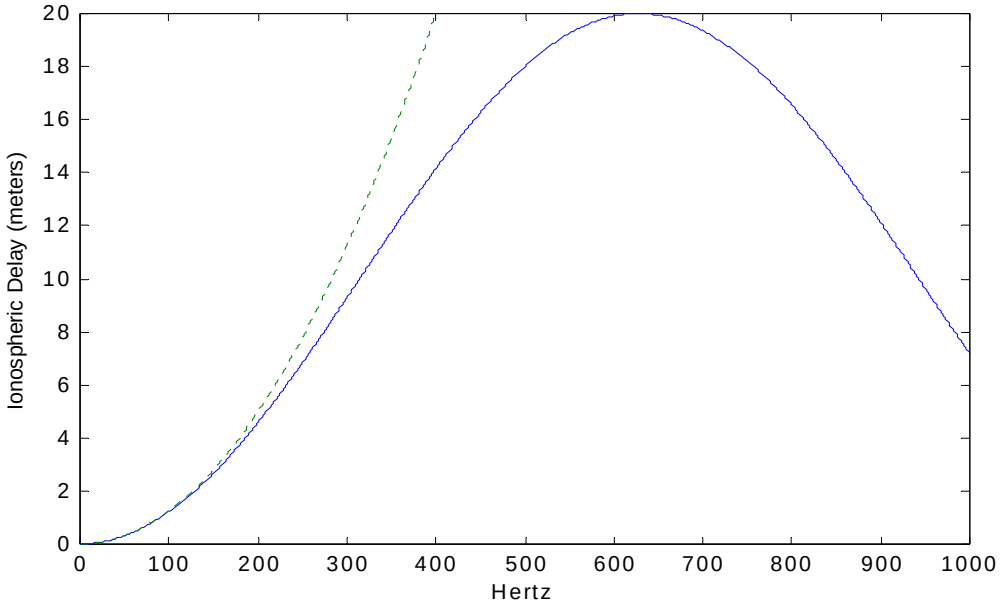

Figure 4.8. Parabola Approximated by a Sinusoid

4.4 Response to a Sinusoidal Input

This analysis will be started by examining the response of several filters initialized at different times in Figure 4.9. Examining the plot, the error does not always increase with k_o like in the previous cases. In fact the initial error is periodic like the input. This important observation leads to the fact that k_o is no longer a directly contributing parameter in the ranging error. What does contribute to the error is the modulus of k_o/T. This value determines at what phase relative of the input the aircraft initializes and furthermore bounds the initial error for a given frequency. To simplify the analysis a bit, if we assume a worst case initialization angle for a given frequency, then the ranging error depends solely on the input frequency and the maximum absolute Ionospheric delay. To see this the solution of the response of the Hatch filter with a sinusoidal input must be attained. The input will be a scaled cosine with some frequency. Since only the rates are of interest it does not matter if the input oscillates about zero.

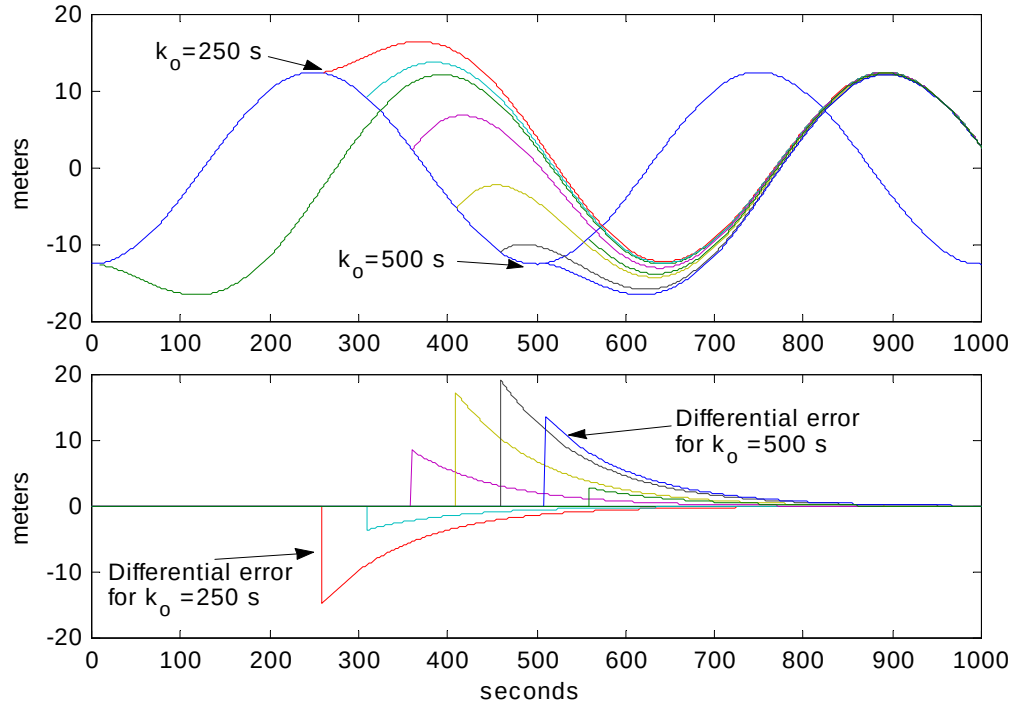

Figure 4.9. Response of Hatch Filters Initialized at Different Times

The input and its z-transform are,

$$i(kT) = \frac{I_{\max}}{2}\cos(\omega kT)$$

$$I(z) = \frac{I_{\max}}{2}\left[\frac{1}{2}\frac{z}{z - e^{j\omega kT}} + \frac{1}{2}\frac{z}{z - e^{-j\omega kT}}\right] \tag{4.19}$$

Applying the input and taking the inverse z-transform gives the solution of the Hatch Filter with a sinusoidal input. Applying initial conditions and an initialization difference k_o to the aircraft filter and differencing, the solution for the differential ranging error is given by Equation (4-20).

$$\Delta\delta = \frac{I_{\max}}{2}\left[\frac{A+B}{C} - \sin(\omega k_o T)\right]\left(\frac{\tau - T}{\tau}\right)^{k-k_o} \tag{4-20}$$

where

$$A = 2T\sin(\omega T)(\tau - T)\cos(k_o \omega T)$$

$$B = \left[2(\tau - T)^2(1 - \cos(\omega T)) - T^2\right]\sin(k_o \omega T)$$

$$C = T^2 + 2\tau(\tau - T)(1 - \cos(\omega T))$$

To find the initialization time difference that corresponds to a worst case phase shift, the first term of Equation (4-20) is differentiated with respect to k_o and solved for k_o.

$$k_{o\_wc} = \frac{\arctan\left[\frac{\sin(\omega T)}{T}\frac{(2\tau - T)}{(\cos(\omega T)+1)}\right]}{\omega T} \approx \frac{\arctan(\omega\tau)}{\omega T} \tag{4-21}$$

Using Equation (4-21) in Equation (4-20), the differential ranging error can be parameterized to yield

$$\frac{2\Delta\delta}{I_{\max}} = \left[\frac{A+B}{C} - \sin(\omega k_{o\_wc} T)\right]\left(\frac{\tau - T}{\tau}\right)^{k-k_o} \tag{4-22}$$

This equation will be plotted like the previous parameterized curves but now with $2\Delta\delta/I_{max}$ on the Y axis, the wait time $(k-k_o)T$ as before and the input frequency as the parameter. The feature that makes this equation useful is that it is bounded as the input frequency increases. If we take the limit of Equation (4-22) as ω approaches 1Hz, half the sampling frequency, we are left with a worst case curve. These curves are plotted on Figure 4.10. This plot is interpreted in the same manner as all the previous parametric plots. For example, consider finding the wait time for a sinusoidal input of unknown frequency and a maximum Ionospheric delay of 25 meters to impose a differential ranging error of no more than .1 meters. First the parameterized differential ranging error is .1/25=.004. Since the input frequency is unknown the worst case curve of $\omega=1/2\pi$ must be used. This is half the sampling frequency of the filter. Frequencies higher than this cannot be detected by the filter. For these parameters the minimum wait from the plot is approximately 600 seconds. Though this worst case value is much higher than that

of found in the ramp analysis, it is a bounded value, unlike the results found in the parabolic analysis. The sinusoidal model is superior because it models the bounded physical process (Ionosphere).

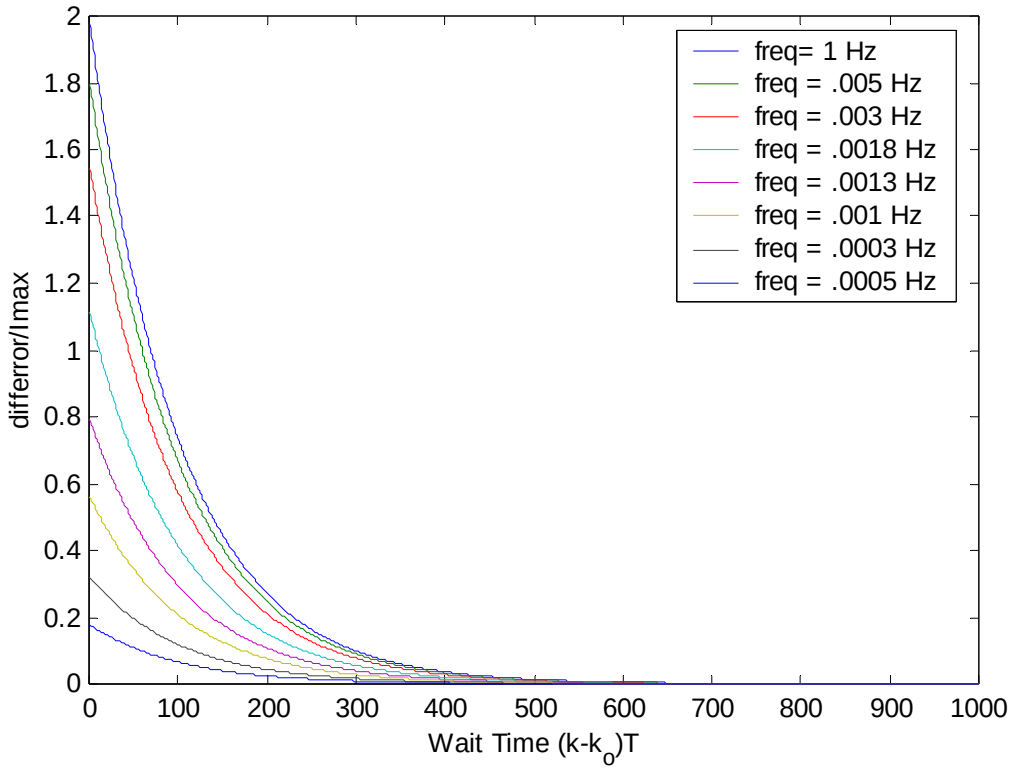

Figure 4.11. Parameterized Curves for Periodic Divergence with Varying Initialization Times

4.5 Discussion

The time domain analysis in this chapter assumed identical filters with a common input but different initialization times. The three inputs were first order, second order and sinusoidal input. The response to third order curves was very similar to that of second order curves and is analyzed in Appendix A. For the first order input, it was found that for given a_1 value and safety limit $\Delta\delta$, there is a minimum required wait time independent

of the initialization time difference. This is a useful result in the LAAS architecture because at no time will the k_o be known by the ground receiver or aircraft receiver. This result was and still will be a benchmark in the analysis of the filters with higher order inputs.

In the analysis with a second order input, the first problem presented is that the ranging error will never reach a steady state value. Therefore a sufficient wait time cannot be specifically defined. However, it is not physically possible for the Ionosphere to sustain a constant parabolic and higher order inputs for long durations. When the magnitude of the delay has reached the Ionosphere maximum, either the divergence will vanish or change directions (converge). Either way the growth of the error will cease. This action shed new light on the problem of bounding the parabolic input. It also revealed that the input may be better modeled by a sinusoidal wave with some random frequency. For this reason a frequency analysis was conducted to try and find bounding features of either the input or the initialization difference. The frequency analysis showed that the initialization error is a function of only initialization angle (phase). Using a worst case initialization angle and frequency for all inputs, the minimum wait time was expressed as a function of the specified differential ranging error limit and the maximum Ionospheric delay only.

CHAPTER V

ANALYSIS WITH TIME CONSTANT DIFFERENCE

In this chapter we consider ground and aircraft filters with different time constants but no difference in initialization time. The differential ranging error will start out at zero and increase with time, opposite of what was witnessed in the previous chapter. As will be seen the time domain analysis that was conducted in the previous chapter will not be sufficient for higher order inputs. Instead, the higher order analysis will be conducted in the frequency domain

5.1 Response to Ramp Input

Currently in the United States there are no restrictions on the aircraft filter time constant, but a requirement of 100 seconds is set for the ground filters [FAA99]. In this situation, not only will the multipath be filtered differently, but the errors induced by the Ionosphere will not be identical. This differential error is present in a DGPS scenario and can potentially reduce the integrity of the system. The analysis will start by examining the differential error due to ramp Ionospheric divergences. From Equation (3-17) it is immediately known that there will be a steady state error due to a ramp input.

$$2a_1\left(\tau_g - \tau_a\right)$$

The steady state error is dependent on the rate of the divergence, a_1, and the difference in time constants $\Delta\tau=\tau_g-\tau_a$. Differencing the analytic solutions due to a ramp input (Equation (4-6)) for the ground and aircraft filters yields the differential response of the filters:

$$\Delta\delta = a_1\left[2\Delta\tau - 2(\tau_g - T)\left(1-\frac{T}{\tau_g}\right)^k + 2(\tau_g - \Delta\tau - T)\left(1-\frac{T}{\tau_g-\Delta\tau}\right)^k\right] \qquad (5\text{-}1)$$

For general use of (5-1) it is parameterized in a similar way that was done in the previous chapter. The parameterized response is

$$\frac{\Delta\delta}{a_1\tau_g} = 2\frac{\Delta\tau}{\tau_g} - 2\left(1-\frac{T}{\tau_g}\right)\left(1-\frac{T}{\tau_g}\right)^{\frac{kT}{\tau_g}\frac{\tau_g}{T}} + 2\left(1-\frac{\Delta\tau}{\tau_g}-\frac{T}{\tau_g}\right)\left(1-\frac{\frac{T}{\tau_g}}{1-\frac{\Delta\tau}{\tau_g}}\right)^{\frac{kT}{\tau_g}\frac{\tau_g}{T}} \qquad (5\text{-}2)$$

Plotting these curves for different $\Delta\tau$'s in Figure 5.1 provides a visual aid for the response sought.

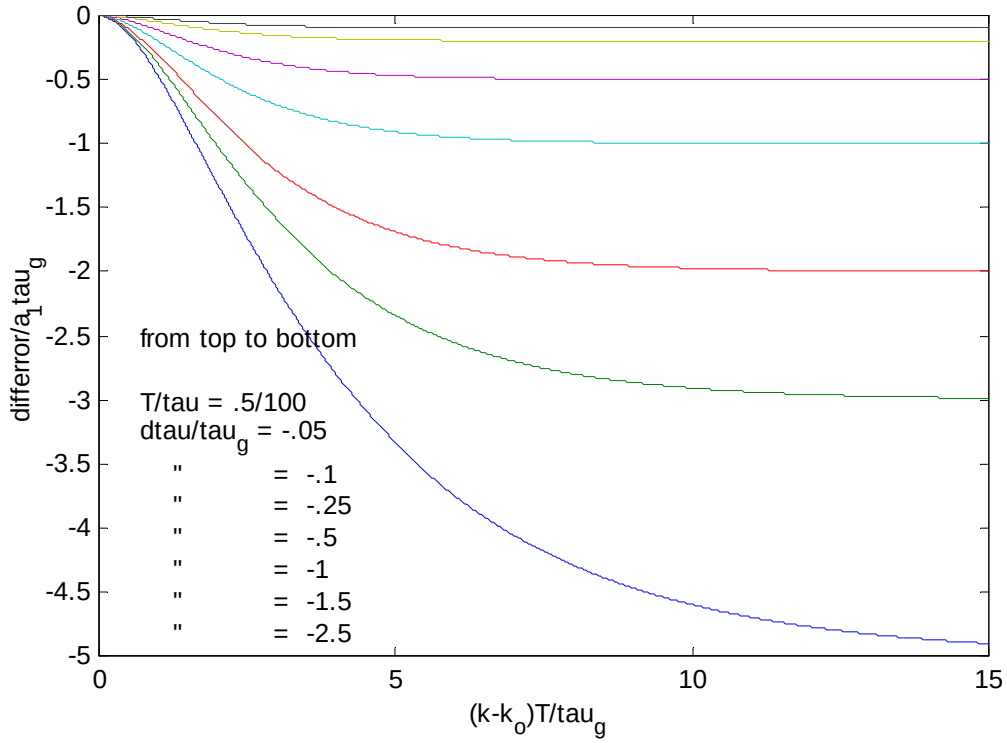

Figure 5.1. Parameterized Curves for Filters with Mismatched Time Constants and Ramp Input

Examining Figure 5.1, the differential ranging error starts at zero and grows to its steady state value. The error at any time after the filters have initialized is found the same way as in the previous chapter. For example, using the prescribed values for the ground filter and ramp divergence in the previous chapter, if the differential ranging error after 500 seconds is sought for an aircraft filter with time constant τ_a=125, the following steps must be taken. First calculate the parameterized value for the time constant difference and the parameterized time elapsed after initialization.

$$\frac{\Delta\tau}{\tau_g} = \frac{\tau_g - \tau_a}{\tau_g} = \frac{100-125}{100} = -.25 \tag{5-3}$$

This value corresponds to one of the curves on the plot. The curves define the relationship between the elapsed time and the differential error. In this example the parameterized error is

$$\delta = -.47 a_1 \tau_g = -.47(.01)(100) = -.47 \text{ meters} \tag{5-4}$$

This value happens to be above the tolerable differential error value of .1 meters for a ramp input of .01m/s and furthermore, by examining the plot, it is clear that the error has not yet reached its steady state value. To find the final error with these values directly, Equation (3-17) will be used.

$$\delta = 2a_1(\Delta\tau) = 2(.01)(-25) = -.5 \text{ meters} \tag{5-5}$$

To find the maximum tolerable $\Delta\tau$ for the given input and error limit, use of Equation (3-17) is made again to yield

$$\Delta\tau = \frac{\delta}{2a_1} = \frac{.10}{2(.01)} = 5 \text{ seconds} \tag{5.6}$$

This is the value for which the aircraft filter time constant can vary from the ground time constant filter and be under the differential error limit. The next section shows that a parabolic input to filters with mismatched time constants will not only cause an error of larger magnitude but one that will not converge to a steady state value.

5.2 Response to a Parabolic Input

From existing collected data, it is known that parabolic divergences do in fact exist. This section will characterize the behavior of the differential ranging error of the filters due to such inputs.

From Equation (3-16), it is seen that the differential error will approach infinity as s approaches zero. This is the final value of the error. The differential ranging error for filters with mismatched time constants and parabolic input is derived from Equation (4-6).

$$\begin{aligned}\Delta\delta = {} & 2a_2\left(\tau_g - \Delta\tau - T\right)\left(T - 2\left(\tau_g - \Delta\tau\right)\right)\left(1 - \frac{T}{\tau_g - \Delta\tau}\right)^k \\ & - 2a_2\left(\tau_g - T\right)\left(T - 2\tau_g\right)\left(1 - \frac{T}{\tau_g}\right)^k + 2a_2\Delta\tau\left(3T + 2\Delta\tau + 2kT - 4\tau_g\right)\end{aligned} \tag{5-7}$$

By inspection of the last term of the above equation, the error will approach infinity as k approaches infinity. Parameterizing Equation (5-7) as done in the previous section gives,

$$\begin{aligned}\frac{\Delta\delta}{a_2\tau_g^2} = {} & 2\left(1 - \frac{\Delta\tau}{\tau_g} - \frac{T}{\tau_g}\right)\left(\frac{T}{\tau_g} - 2 + 2\frac{\Delta\tau}{\tau_g}\right)\left(1 - \frac{\frac{T}{\tau_g}}{1 - \frac{\Delta\tau}{\tau_g}}\right)^{k\frac{T}{\tau_g}\frac{\tau_g}{T_g}} \\ & - 2\left(1 - \frac{T}{\tau_g}\right)\left(\frac{T}{\tau_g} - 2\right)\left(1 - \frac{T}{\tau_g}\right)^{k\frac{T}{\tau_g}\frac{\tau_g}{T_g}} + 2\frac{\Delta\tau}{\tau_g}\left(3\frac{T}{\tau_g} + 2\frac{\Delta\tau}{\tau_g} + 2\frac{kT}{\tau_g} - 4\right)\end{aligned} \tag{5-8}$$

The result is plotted in Figure 5.2 for various values of $\Delta\tau/\tau_g$.

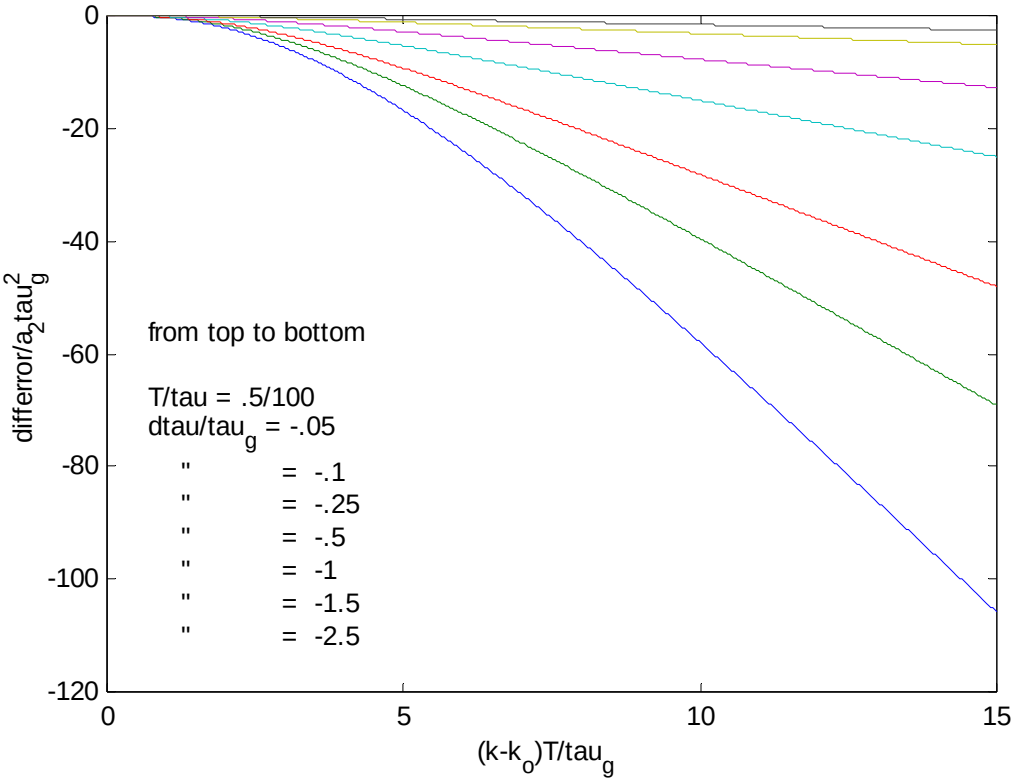

Figure 5.2. Parameterized Curves for Filters with Mismatched Time Constants and Parabolic Input.

Figure 5.2 confirms again that the differential error will approach infinity. Using a $\Delta\tau$ = 5 s, which was found to be acceptable for ramp inputs in the previous section, we are faced with the same problem as in Chapter 4, choosing a worst case a_2 value. Even if a worst case a_2 is supposed, the only information on Figure 5.2 that can be extracted is the time that such a value can be sustained before the differential ranging error exceeds the safety limit. Without knowledge of how long the sustain time actually is, no useful information on the differential error can be found.

Figure 5.3 shows the effect of two running Hatch filters with mismatched time constants tracking a real Ionospheric divergence input. Here the parabolas do not inflate the differential ranging error but seemingly correct it. These experimental results seem to contradict what was gathered from the analysis above. The reason is the analytic solution considered parabolic inputs that start at their minimum and increase with time.

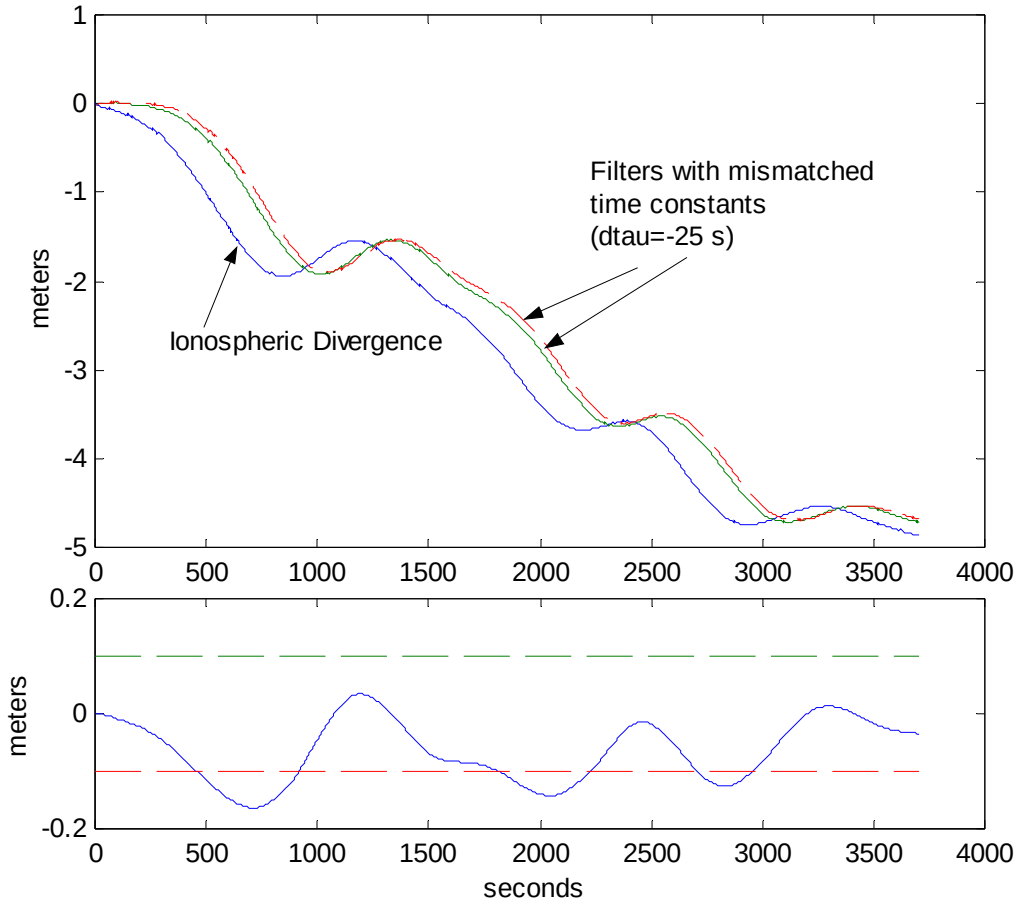

Figure 5.3. Filters Tracking Real Ionospheric Data and the Differential Error

However, the collected data shows that the Ionosphere is cyclic in nature. This may be interpreted in the context of the parabolic analysis as oppositely signed pairs that create local extrema (peaks and troughs) on given intervals. These extrema are points where the

Ionosphere changes directions. The periodic direction changes in the Ionosphere result in a smaller differential error than predicted by the analytical results for a single parabolic input. One other feature seen in Figure 5.3 is that the individual filter outputs lag the input. These observations strongly suggest that additional information about the behavior of the output may be extracted from a frequency analysis.

5.3 Frequency Analysis

This analysis will be conducted in the frequency domain. To begin, the frequency response of the differential output is computed for the frequencies zero to one Hertz. Since the filter is digital it cannot detect frequencies, free of aliases, above half of its own sampling frequency. This is called its Nyquist Frequency. To find the frequency response, the filter will be converted to the frequency domain by replacing every variable z in Equation (4-3) with exp(jωT). Equation (4-3) is then differenced for the ground and air to give the frequency response of the differential error output. After this conversion and differencing, the filter takes the following form:

$$\frac{\left(T-2\tau_g\right)e^{j\omega T}-\tau_g+T}{\tau_g e^{j\omega T}-\tau_g+T}-\frac{\left(T-2\tau_a\right)e^{j\omega T}-\tau_a+T}{\tau_a e^{j\omega T}-\tau_a+T} \tag{5.9}$$

The continuous version of the response is identical to the discrete version except at and near the filters' Nyquist frequency. The continuous equation for the frequency response of the differential error is

$$\frac{2\Delta\tau j\omega}{\tau_g\tau_a\left(j\omega\right)^2+\left(\tau_g+\tau_a\right)j\omega+1} \tag{5-10}$$

The frequency response is displayed by simply plotting the magnitude of Equation (5.10) verses jω. This is a band pass filter with center frequency at and $\omega_{center} = \frac{1}{\sqrt{\tau_g \tau_a}}$. Figure 5.4 shows the frequency responses of both the discrete and continuous differential error. As can be seen the continuous approximation is identical until the frequencies approach the limit of the discrete filter. In this analysis (unlike the frequency analysis conducted in Chapter 3), the phase shift of the differential error is not significant and will not be considered. All the information needed can be found in the gain plot.

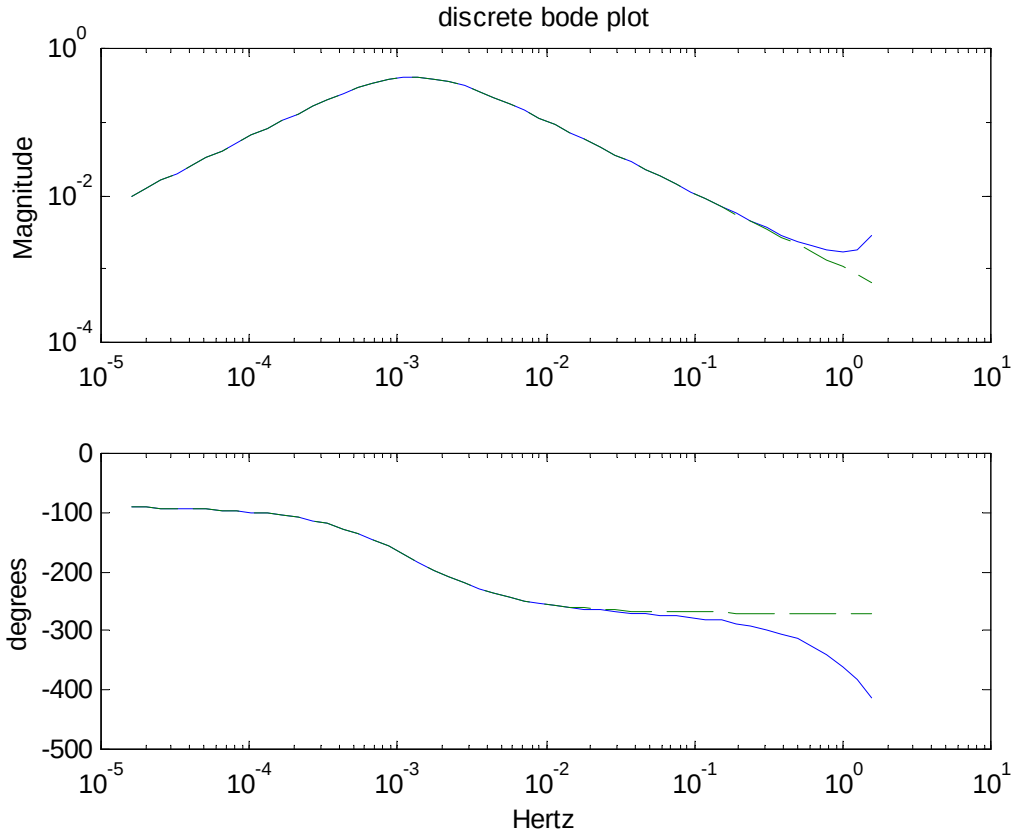

Figure 5.4. Frequency Response of Continuous (dashed line) and Discrete (solid line) Filters

The frequency response of filters with several different values of $\Delta\tau$ are plotted in Figure 5.5. As $\Delta\tau$ decreases the gain of the filters does as well. If $\Delta\tau$ is zero there would be no differential ranging error. The gain is also very small at extremely low frequencies (0 to 10^{-5} Hz) and frequencies that approach the filters' Nyquist frequency. This is an important observation. It shows that the differential ranging error does not respond to low or high frequencies due to the band pass nature of the filter. This is advantageous in that a large portion of the frequency content of Ionosheric divergence will not induce an error in the filter outputs.

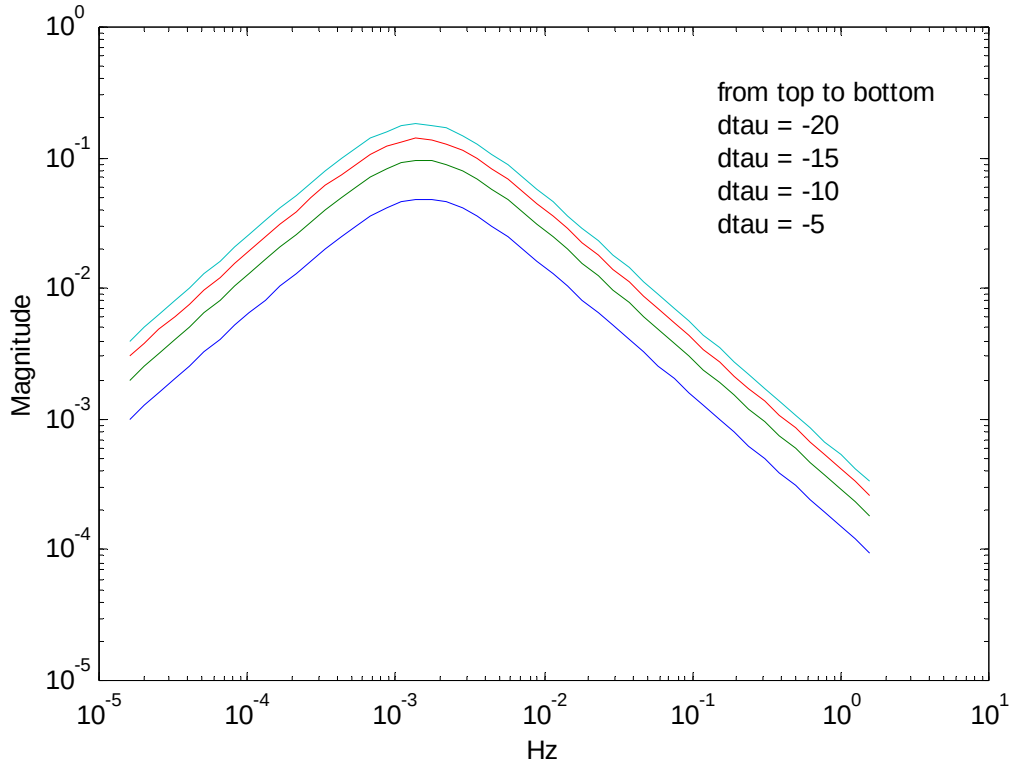

Figure 5.5. Frequency Response of Filters with Mismatched Time Constants

To investigate these ideas consider the equation for the differential ranging error as a function of frequency.

$$\Delta\delta(j\omega) = H(j\omega)I(j\omega) \tag{5-11}$$

Where H(jω) is the frequency response of the differential filter output, I(jω) is the Fourier Transform of the Ionospheric input and Δδ(jω) is the frequency content of the differential ranging error. The tolerable amplitude of the Ionosphere for given frequencies can be found by solving for I(jω) in Equation (5-11) and substituting in values for Δτ and Δδ. For example, if Δτ=15 seconds and Δδ =.1 meters, a plot of the tolerable amplitude of the Ionosphere verses frequency is seen on Figure 5.6 .

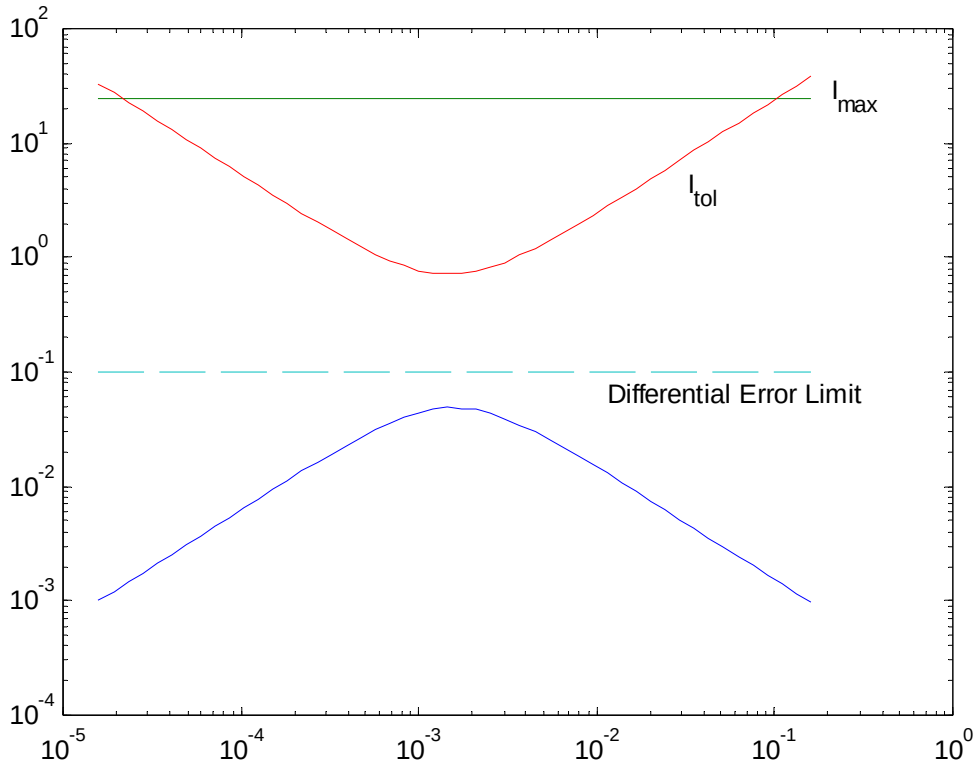

Figure 5.6. Tolerable Amplitude of Ionosphere for Given Frequencies

The top curve in this plot shows the tolerable amplitude for a given input frequency. Anything under this curve will not induce an error larger than the specified limit. If a

maximum Ionospheric delay assumption is plotted as well, the frequencies to the left and right of the left and right intersections of the tolerable Ionosphere and the maximum Ionosphere will never induce an error. An error will exist, however, if the amplitude of a particular frequency lands in the area bounded by the tolerable Ionosphere and maximum Ionosphere curves. This area can be decreased in several different ways. First, the assumed maximum Ionospheric delay can be reduced. However, due to the variable nature of the Ionosphere this value should be kept as conservative as possible (unchanged). Another way is to raise the tolerable amplitude curve. This can be accomplished by either increasing $\Delta\delta$ or decreasing $\Delta\tau$. Since $\Delta\delta$ will be set by requirement, decreasing $\Delta\tau$ is the logical choice for mitigating the differential error. To simplify the above explanation, we can require that the amplitude at any frequency be below the minimum tolerable amplitude. The minimum tolerable amplitude occurs at the frequency that produces maximum gain of the differential filter response. This peak frequency is found by differentiating Equation (5-10) and solving for ω_{peak}. The peak frequency is

$$\omega_{peak} = \frac{1}{\sqrt{\tau_g \tau_a}} \tag{5-12}$$

Substituting Equation (5-12) into Equation (5-10) gives the maximum gain of the differential filter.

$$H\left(j\omega_{peak}\right) = \frac{2\Delta\tau}{2\tau_g - \Delta\tau} \tag{5-13}$$

$I_{tolerable}$ (ω_{peak}) is found by substituting Equation (5-13) into (5-11). This yields a value for which the amplitude of the Ionosphere must be under to not induce a differential ranging error.

$$I_{tolerable} = \frac{\Delta\delta}{\left|H\left(j\omega_{peak}\right)\right|} \tag{5-14}$$

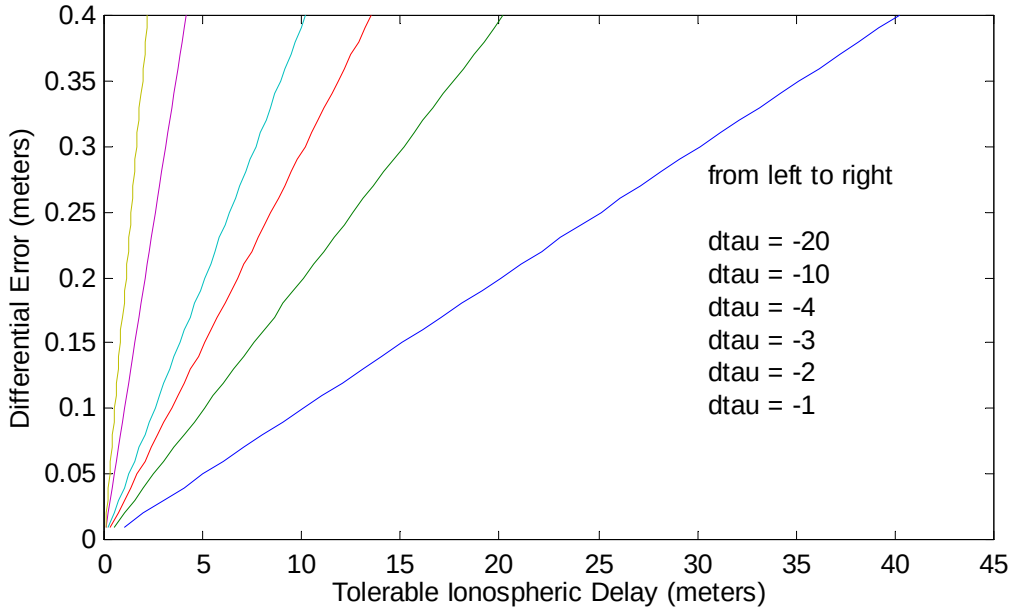

Figure 5.7. Tolerable Amplitude of Ionosphere for Given Safety Limits

This value depends on $\Delta\delta$ and $\Delta\tau$. Equation (5-13) is easily parameterized by letting $\Delta\tau$ be the parameter and letting the tolerable amplitude of the Ionosphere be a function of $\Delta\delta$. These curves are plotted in Figure 5.7. These curves all suggest that $\Delta\tau$ should equal zero for the output error to be a minimum.

To further investigate these ideas, the frequency response of the real ionospheric data will be plotted examined. In Figure 5.8 several Ionospheric divergence traces and their frequency contents are displayed. The frequency contents are obtained by performing a Fast Fourier Transform on the data.

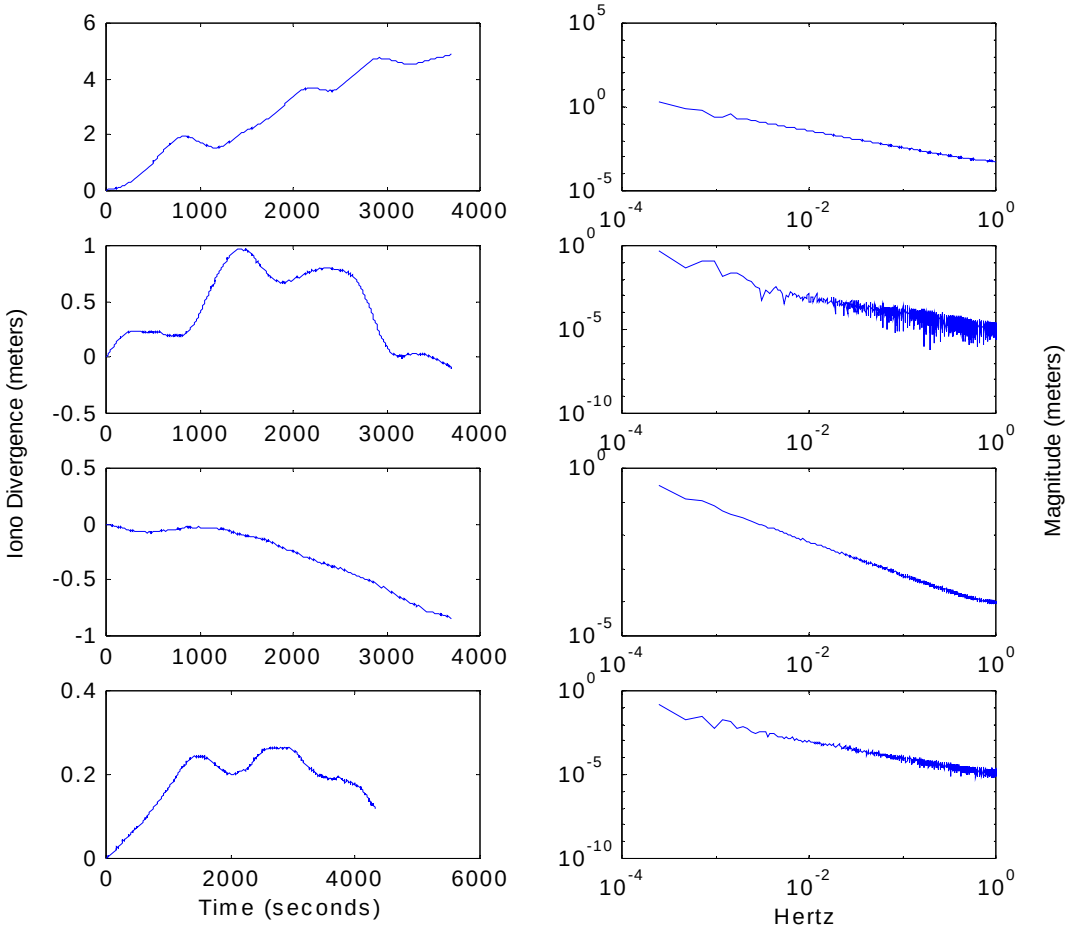

Figure 5.8. Ionospheric Divergences and their Frequency Contents (fft)

By inspection of the plots it is evident that these divergence plots contain primarily very low frequency components. To put the data in perspective, the plots of the frequency domain input are superimposed on the frequency response plots of the filters. Each plot will have filters with several different values of $\Delta\tau$. The actual time domain ranging error will be plotted as well in Figure 5.9. As may have been expected, the filters with higher values of $\Delta\tau$ produce higher error values. In general, the frequency content of the Ionosphere is similar across data sets (Figure 5.10). It is seen that the highest amplitude

of any of these plots is approximately two meters due to the short time relatively short time span (two hours) of each data set.

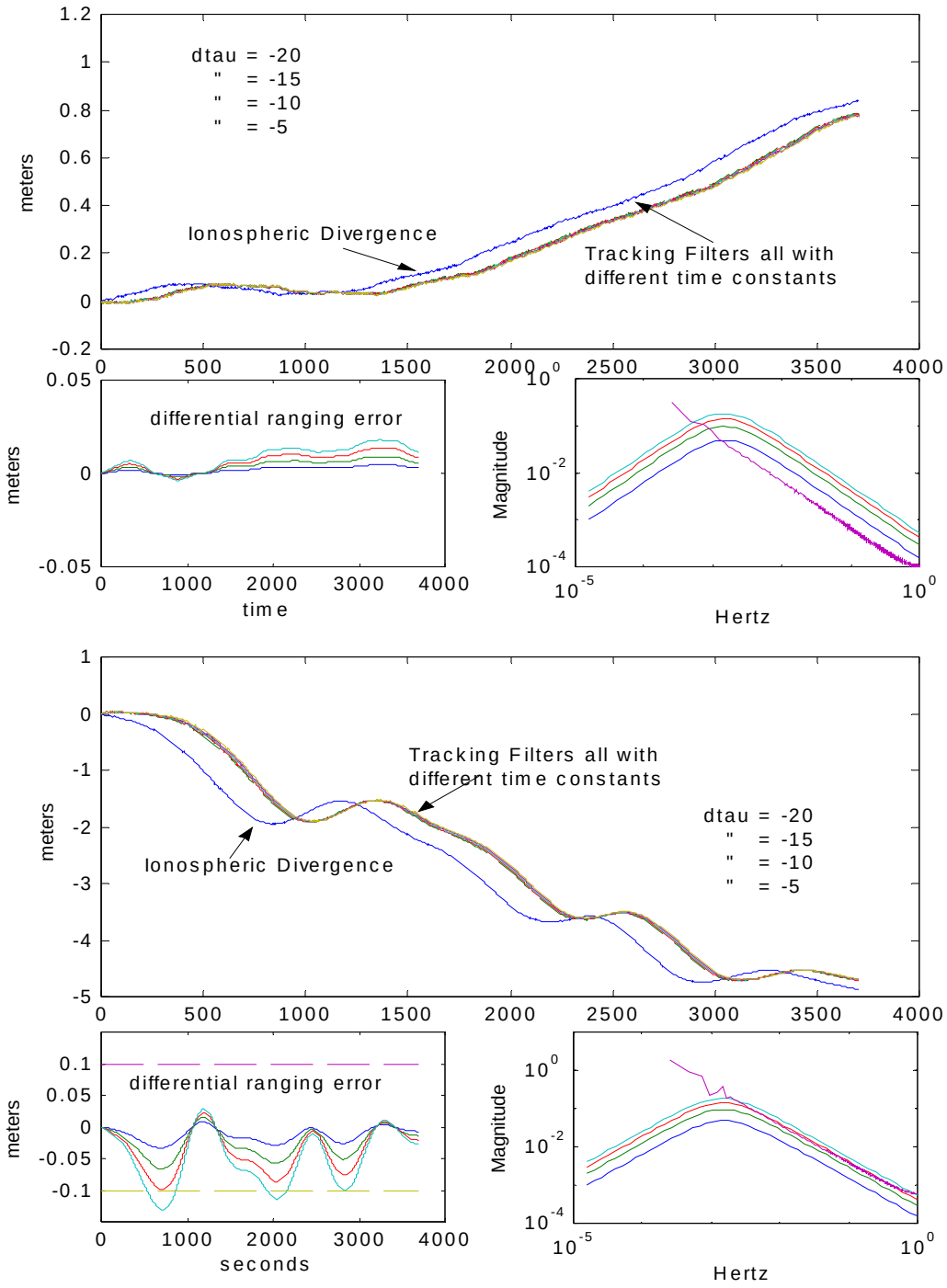

Figure 5.9. (1) Ionospheric Divergence Input with Running Filters, Differential Ranging Error, Frequency Response

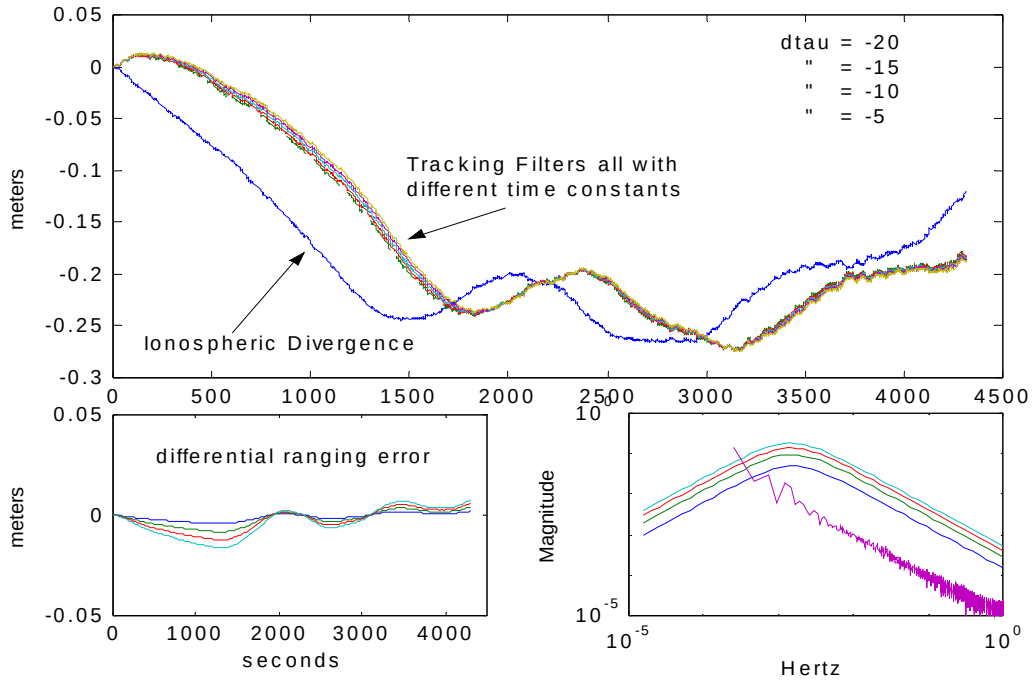

Figure 5.9. (2) Ionospheric Divergence Input with Running Filters, Differential Ranging Error, Frequency

To find the a value for $\Delta\tau$ that will ensure a differential ranging error within specified limits for this particular input, we can use Figure 5.7. For example, if $\Delta\tau$ for a system was sought for a maximum differential ranging error of .1 meters the following steps must be taken. First, the maximum amplitude, irrespective of frequency, is found. From above it was determined to be two meters. A vertical line drawn from this value shall intersect the horizontal line drawn from the specified $\Delta\delta$. The curve that intersects this point is the value for $\Delta\tau$. The value for $\Delta\tau$ is approximately –4 seconds. So, using the highest amplitude from the data set in Figure 5.10, for there never to be a differential ranging error above .1 meters, $\Delta\tau$ should be no less than –4 seconds. To test the accuracy of the method just used, the Ionospheric data set from which the two meter amplitude was found will be applied to the filter via Equation (5-11).

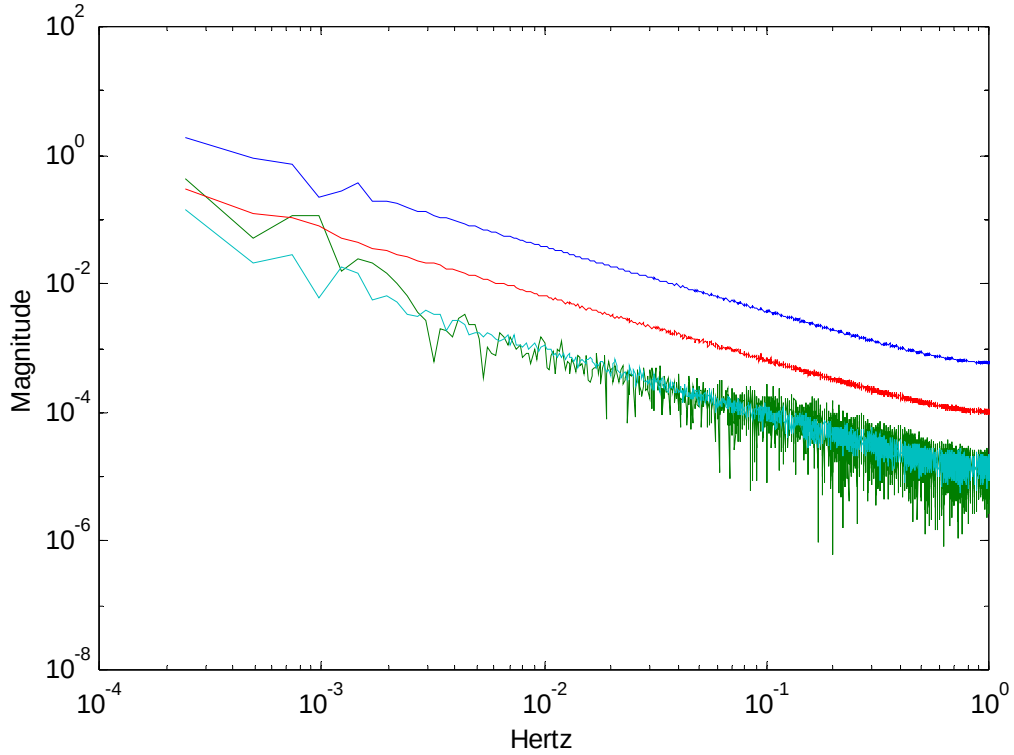

Figure 5.10. Frequency Content of Several Real Ionospheric Divergence Data Sets

The output is the frequency content of the differential ranging error. The data was applied to four filters with $\Delta\tau$ values of –5, -10, -15 and –25 seconds and plotted on Figure 5.11. By inspection of this plot, it is evident that $\Delta\tau$ values of –5 and -10 seconds do not induce an error. These values are not much higher (relative to the 100 second time constant) than the –4 second limit found by using Figure 5.7. This is because it is assumed that the maximum amplitude occurs at the peak gain of the filter. The method of Figure 5.7 also assumes that the input is only a tone frequency. This method is deliberately conservative because of the unpredictability of the Ionosphere, but as seen yields values ($\Delta\tau$=-4 seconds) that are not far from maximum physical values that do not induce an error ($\Delta\tau$=-10 seconds).

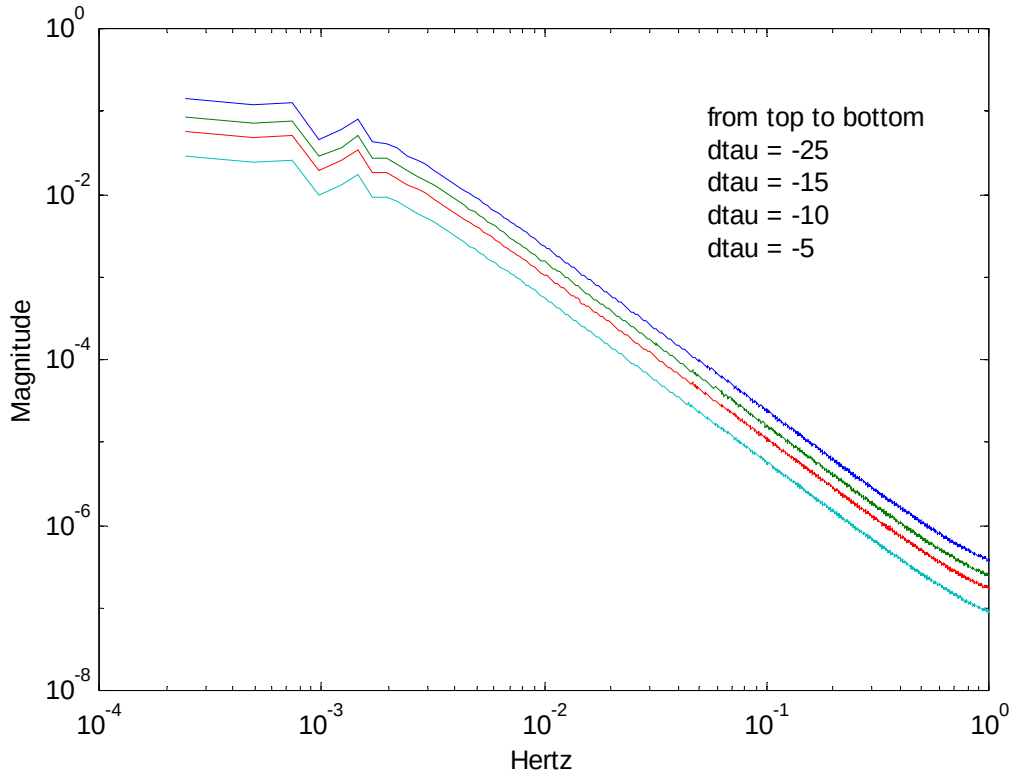

Figure 5.11. Frequency Content of Differential Ranging Error

5.4 Discussion

From the preceding analysis it is seen that if a $\Delta\tau$ exists a differential error will also exist. The magnitude and nature of the error will depend on the size and shape of the Ionospheric divergence input. For the ramp case, the steady state differential error can be found immediately by Equation (3-17). From this equation a maximum value for $\Delta\tau$ can be found as well for a given input. For inputs of higher order, however, the differential error would increase without bound for as long as the input was sustained. To help analyze the higher order inputs frequency domain analysis was used. This analysis showed that the differential error is a function only of the amplitude and frequency in the input. Figure 4.6 shows that depending on the $\Delta\tau$, $\Delta\delta$ and maximum Ionospheric delay,

some frequencies will never induce an error. The most direct and feasible way to increase the spectrum of these "safe" frequencies is to decrease $\Delta\tau$. The relationship between $\Delta\tau$ and the maximum amplitude of the input irrespective of frequency is found in Figure 4.7. These results were shown to be slightly conservative when compared with results obtained from direct filtering of Ionospheric divergence data. The assumptions made by this method are that the maximum amplitude of the Ionosphere occurs at the peak gain of the filter and that the input is a tone frequency. From the experimental data, we know this not generally the case. The total power of the signal is spread throughout the spectrum and is generally unknown.

To handle multiple frequencies with varying amplitude (or power), a different approach must be taken. One candidate approach is to treat the Ionospheric divergence as a random signal. In this case, it can be analyzed using its power spectral and statistical properties. The "Future Work" section in the summary chapter presents a plan of attack to carry this analysis out.

From the values and the variable nature of the Ionosphere, it is evident that even a small difference in the value of the time constants of the ground and air filters could easily cause unacceptable errors. This high-risk sensitivity does not seem worth the prize of having the freedom to use a slightly different aircraft time constant from that of the required ground time constant. Although there are other factors that influence the choice of the time constant, the obvious solution to mitigating the differential ranging error due to $\Delta\tau$ is for $\Delta\tau$ to equal to zero.

CHAPTER VI

SUMMARY

6.1 Summary of Results for Initialization Time Difference

The first analysis conducted (Chapter 4) characterized the differential ranging error as a function of initialization time difference with respect to Ionospheric Divergence. The analysis started by modeling the Ionosphere as a ramp. The results showed that ramp inputs will induce a differential ranging error between the two filters but that the error is bounded. From experimental data, however, it is clear that the Ionosphere contains features that are not strictly ramp like. For this reason the analysis was extended using a parabolic model. Since identical filters were used in this analysis, the differential ranging error due to an initialization time difference would eventually decay to zero, but the time needed to do so was not bounded. This new difficulty arises from the fact that the input is second order and the Hatch filter is first order. This will cause the initial error to increase for as long as the second order input is sustained. Without having knowledge of the initialization time difference, the initial error is unknown and as a result the convergence time is unknown, unlike the previous ramp analysis. This analysis was not able to provide useful information about the differential ranging error. From real Ionospheric divergence data, however, it was easy to see that a polynomial of any order (with positive coefficients) could not be sustained indefinitely. Because the parabolic model is not bounded, it will not accurately model the Ionosphere. From this fact rose the concept of the frequency model of the Ionosphere.

The analysis then focused on using a sinusoidal input for the Ionosphere. It was found that the differential ranging error depended on the input frequency, amplitude and

initialization phase shift of the second filter (assuming the first filter had reached steady state), all of which were boundable. This approach did provide useful results (like the ramp analysis) because the maximum error was bounded. The results of this analysis are summarized in Table 6.1.

Table 6.1 Summary of Results for Initialization Time Difference

Model	Bounding Attribute	Unknown Parameter	Results
Ramp	k_o	a_1	Max error bounded (e.g. 300 s wait time)
Parabolic	none	a_2	Error not bounded Not a useful physical model
Frequency	ω,θ	I_{max}	Max error bounded (e.g. 600 s wait time)

A common result from all the above models is that the errors all decay at the same rate:

$$\left(\frac{\tau - T}{\tau}\right)^k$$

From these results necessary and sufficient conditions are defined. Sufficient conditions to ensure the safe interoperability between identical filters with an initialization time difference in DGPS are as follows:

1) Define acceptable wait time using direct method applied to ramp and harmonic models.
2) Define acceptable inflated standard deviation (σ) of range measurement error as a function of time using ramp or harmonic models.

The necessary condition to ensure the safe interoperability between identical filters with an initialization time difference in DGPS is as follows:

1) Any mechanism used to weight or de-weight values associated with the filter outputs must have dynamics no faster than:

$$\left(\frac{\tau - T}{\tau}\right)^k$$

6.2 Summary of Results for Mismatched Time Constants

The second set of analysis conducted (Chapter 5) characterized the differential ranging error as a function of the filter time constant differences with respect to Ionospheric Divergence. The results of this analysis differed from the previous one in that the differential ranging error did not decay with time. This was seen immediately using the ramp model. With this first order input the differential ranging error converged to a nonzero steady state value. On the other hand, the second order input produced a differential ranging error that increased for as long as the input was sustained. Since the parabolic input, as mentioned before, was not a good physical model, a sinusoidal model was used instead and a frequency response analysis was performed. The first observation of the differential filter is that it behaved like a band pass filter. The differential filter would reject high and low frequencies but still had considerable gain at its peak. As was expected the value of $\Delta\tau$ controlled the gain, which in turn controlled the magnitude of the error. Since τ_g is specified at a required value (100 s) $\Delta\tau$ will presumably be known. If $\Delta\tau$ is known, the tolerable amplitude at a single frequency could be found. Using the assumption that the Ionospheric delay has an absolute maximum value, the tolerable

amplitudes at the extreme high and low frequencies are higher than the maximum amplitude, therefore never inducing an error. However, the amplitudes near the peak gain frequency could induce an error easily. The results are summarized in Table 6.2.

Table 6.2 Summary of Results for Filters with Mismatched Time Constants

Model	Bounding Attribute	Parameter	Results
Ramp	a_1	$\Delta\tau$	Steady State Defined
Parabolic	none	$\Delta\tau$	Errors will increase for as long as input is sustained
Frequency	I_{max}	$\Delta\tau$	Errors are bounded

A common result from all the above models in this analysis is that the errors all depend on $\Delta\tau$. From these results necessary and sufficient conditions are defined. Sufficient conditions to ensure the safe interoperability between filters with mismatched time constants in DGPS are as follows:

1) Let $\Delta\tau = 0$.

2) Some tolerance may be possible (but small). Can define maximum time constant difference from above quantified results to ensure there is no differential ranging error.

3) Define inflated standard deviation (σ) scaled with the derived quantity:

$$\frac{2\Delta\tau}{2\tau_g - \Delta\tau}$$

The necessary condition to ensure the safe interoperability between filters with mismatched time constants in DGPS is as follows:

1) Any mechanism used to weight or de-weight value associated with the filter outputs must be scaled with the maximum gain of the differential filter:

$$\frac{2\Delta\tau}{2\tau_g - \Delta\tau}$$

6.3 Future Work

The above frequency analysis is valid only for single harmonic inputs. However, from collected experimental data, it is known that the spectral content of the Ionospheric error is not localized to any individual frequency. Because of the highly variable nature of the Ionosphere, the frequency content will generally not be known in advance, and Ionosphere may be treated as a stochastic process. In the stochastic case, instead of dealing with ramp and frequency magnitudes and differential error, the new inputs and outputs are Power Spectral Densities (PSD) and variances. Specifically, the PSD of the differential error is related to the differential filter and the PSD of the Ionosphere as follows:

$$S_e(\omega) = |H(\omega)|^2 S_I(\omega) \tag{6-1}$$

When the PSD of the output is obtained the variance of the output can be found by

$$\sigma_e^2 = \int_{-\infty}^{\infty} S_e(\omega) d\omega \tag{6-2}$$

The standard deviation of the output if easily obtained by taking the square root of the variance. This standard deviation is analogous to the differential ranging error ($\Delta\delta$) used

throughout the previous analyses and can be used as the end requirement that must be met.

With sufficient data collected, a Gauss Markov Random Process model can be assigned to the Ionosphere. To obtain such a model data must be collected from different times in the day throughout the year and at different locations.

APPENDIX

APPENDIX

RESPONSE TO A CUBIC INPUT

In this Appendix, the differential response of ground and aircraft filters with an initialization time difference and a third order input will be examined. The analysis will show that the differential ranging error induced by a third order Ionospheric input is unbounded for as long as the input is sustained and grows rapidly. It is the intention of this analysis to show that simulating higher order inputs offer little that could not be deduced from second order input analysis.

The third order input induces a growing error that increases at a second order rate. To conduct the analysis, we must apply initial conditions to Equation (4-6) and difference for the ground and air. The initial conditions are found a bit differently for the third order input. Here we will equate the third order input equation as a function of kT with the third order input equation as a function of $(k-k_o)T$ and find the coefficients of the initial conditions by inspection. The equivalent functions are

$$a_3 k^3 T^3 = a_3 (k - k_o)^3 T^3 \tag{A-1}$$

Expanding Equation (A-1) gives

$$a_3 k^3 T^3 = a_3 k^3 T^3 - a_3 3(k_o T)(kT)^2 + a_3 3(k_o T)^2 (kT) - a_3 3(k_o T)^3 \tag{A-2}$$

It is easily seen that the values preceding the $(kT)^x$ terms are the coefficients for the step, ramp and parabola initial conditions. As before, the value of the input, a_3, does not change. The initial conditions to be used in the aircraft solution are as follows

$$\begin{aligned} a_3 &= a_3 \\ a_2 &= 3a_3 k_o T \\ a_1 &= 3a_3 (k_o T)^2 \\ a_0 &= 3a_3 (k_o T)^3 \end{aligned} \tag{A-3}$$

Applying the initial conditions and differencing Equation (4-6), the solution of the differential ranging error due to a third order input is

$$\begin{aligned} \Delta\delta = a_3 \left(2T^3 - 14T^2\tau + 24\tau^2 T - 12\tau^3\right)\left(\frac{\tau - T}{\tau}\right)^{kT}\left[1 - \left(\frac{\tau - T}{\tau}\right)^{-k_o T}\right]... \\ - a_3\left(6k_o T\left(T^2 - 3T\tau + 2\tau^2\right)\right) + 6a_3 (k_o T)^2 (\tau - T)\left(\frac{\tau - T}{\tau}\right)^{k - k_o} \end{aligned} \tag{A-4}$$

For analysis, we parameterize this curve like in the previous sections.

$$\begin{aligned} \frac{\Delta\delta}{a_3\tau^3} = \left(2\left(\frac{T}{\tau}\right)^3 - 14\left(\frac{T}{\tau}\right)^2 24\left(\frac{T}{\tau}\right) - 12\right)\left(1 - \frac{T}{\tau}\right)^{\frac{kT}{\tau}\frac{\tau}{T}}\left[1 - \left(1 - \frac{T}{\tau}\right)^{-\frac{k_o T}{\tau}\frac{\tau}{T}}\right] \\ - \left(6k_o \frac{T}{\tau}\left(\left(\frac{T}{\tau}\right)^2 - 3\left(\frac{T}{\tau}\right) + 2\right)\right) + 6\left(k_o \frac{T}{\tau}\right)^2\left(\frac{T}{\tau} - 1\right)\left(1 - \frac{T}{\tau}\right)^{\left(\frac{kT}{\tau} - \frac{k_o T}{\tau}\right)\frac{\tau}{T}} \end{aligned} \tag{A-5}$$

and plot for several different values of k_o. The plot looks very similar to those of the first and second order input plots, only much larger in magnitude for k_o. This input has the same problem of bounding k_o or a_3 as was seen in the second order input analysis. As was stated earlier this, and higher order simulations will not yield information that cannot be deduced from the second order input analysis. Though the plot seems to diminish any hope of the ranging error be within limits, it is physically impossible for an a_3 of dangerous values to be sustained for infinity. This is true because the maximum delay contributed by Ionosphere the at zenith is about 25 meters, and for the Ionosphere to go from one to 25 meters in the form of a parabolic curve, there is a maximum sustain time associated with any particular a_3 value. When the Ionospheric delay reaches its

maximum, it will either remain constant, in which case no differential error will be induced or it will switch directions and begin to decrease.

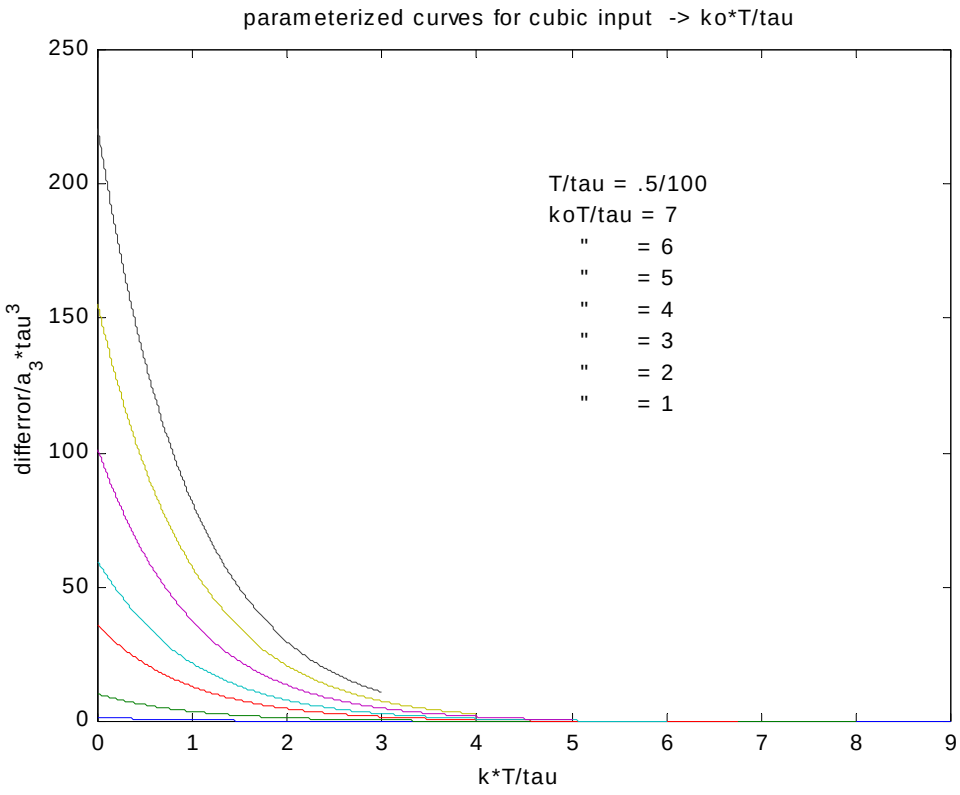

Figure A.1. Parameterized Curve for Cubic Divergence

BIBLIOGRAPHY

[Dav65] Davis, K., Ionospheric Radio Propagation, United States Commerce Department, p. 71, 1965.

[Dor97] Dorhety, P.H., Gendron, P.J., Loh,R., Anderson, D.N., "The Spatial and Temporal Variations in Ionospheric Range Delay", ION GPS-97, pp. 231-240, Sept 1997.

[FAA99] Federal Aviation Administration, Specifications for Performance Type One Local Area Augmentation System Ground Facility, FAA-E-2937, p. 24, 1999

[Hat82] Hatch, R., "The Synergism of GPS code and carrier measurements," Proc. 3rd International Geodetic Symposium Satellite Doppler Positioning, Las Cruces,1982

[Klob86] Klobuchar, J.A., "Design and Characteristics of the GPS Ionospheric Time Delay Algorithm for Single Frequency Users," IEEE, PLANS 1986, Position Location and Navigation Symposium, Record 86 CH 2365-5, pp. 280-286, Nov 1986.

[Klob96] Klobuchar, J.A., "Ionospheric Effects on GPS," Global Positioning System Theories and Applications Volume 1, American Institute of Aeronautics and Astronautics, Inc., p. 509, 1996.

[Lei95] Leick, A., GPS Satellite Surveying, John Wiley and Sons, Inc., 2nd ed., pp. 290-296, 1995.

[MOP99] RTCA, Inc., Minimum Operational Performance Standards for GPS Local Area Augmentation System, Draft 14, p. 33, 1999

[Park94] Parkinson, B.W.,"GPS Error Analysis," Global Positioning System Theories and Applications Volume 1, American Institute of Aeronautics and Astronautics, Inc., pp. 477-481, 1994.

[Park95] Parkinson, B.W.,"Differential GPS," Global Positioning System Theories and Applications Volume 2, American Institute of Aeronautics and Astronautics, Inc., pp. 27-30, 1995.

[Spil94] Spilker, J.J,"Tropospheric Effects on GPS," Global Positioning System Theories and Applications Volume 1, American Institute of Aeronautics and Astronautics, Inc., p. 543, 1994.

[Tas94] Tascione, T.F., Introduction to the Space Environment, Krieger Publishing Company, 2nd ed., p. 89, 1994.

[Van95] Van Dierendonck, A.J., ”GPS Receivers,” Global Positioning System Theories and Applications Volume 1, American Institute of Aeronautics and Astronautics, Inc., p. 333, 1995.

[Zum94] Zumberg, J.F., Bertiger, W.I., ”Ephemeris and Clock Navigation Message Accuracy”, Global Positioning System Theories and Applications Volume 1, American Institute of Aeronautics and Astronautics, Inc., p. 597, 1994.